Recent thermohaline shifts in the Adriatic Sea and their potential consequences

Elena Terzić[1] and Ivica Vilibić[1,2]

[1]Ruđer Bošković Institute, Division for Marine and Environmental Research, Bijenička cesta 54, 10000 Zagreb, Croatia
[2]Institute for Adriatic Crops and Karst Reclamation, Put Duilova 11, 21000 Split, Croatia

Correspondence: Elena Terzić (eterzic@irb.hr)

Abstract. The Adriatic Sea has warmed and salinified rapidly over the past two decades, and the changes are not uniform with depth. We combine 33 664 quality-controlled shipboard and Argo temperature and salinity casts spanning 1950–2025 into two climatologies, and use Argo profiles alone in the Southern Adriatic Pit, to quantify the vertical structure of the change and to test formally for regime shifts. Between the 1950–1999 and 2000–2025 climatologies the southern Adriatic warmed and salinified at every depth and season, by 0.11–0.53 in salinity and up to 1.6 °C in temperature, the only exception being the uppermost levels in summer and autumn, which the two periods sample differently. Amplification relative to the Mediterranean is strongly depth-dependent: below 700 m the southern Adriatic warms at 6.2 times the basin-median rate, whereas above 200 m its warming is not amplified. Near-surface salinity maxima ("surface saline lakes") step up after 2014, in ship and float records alike, from a few per cent of warm-season casts to about 40 %, a regime shift that is demonstrable only once vertical resolution and platform are controlled for. The intermediate salinity maximum has lost its dominant band, and where two maxima coexist they move apart and diverge in density, so they are not one migrating core. Over 2014–2024 the steric contribution in the Southern Adriatic Pit is negative, dominated by halosteric contraction, so that local sea level rise must be mass-driven. Salt fingering has intensified below the classical intermediate core, allowing for salt transport towards deeper layers.

Three consequences follow, set out here as hypotheses. Deep ventilation may persist under milder winters, because water that is already saline needs less cooling to sink; each event may then deliver less oxygen, because the water that sinks is warmer. Exchange of oxygen, nutrients and carbon between the surface and intermediate layers may be either suppressed or enhanced beneath more frequent surface saline lakes, depending on whether stratification or double diffusion prevails. Adriatic ecosystems, in which warming-linked mortality and species redistribution are already documented, face a basin changing faster at depth than at the surface. Testing these hypotheses requires sustained high-resolution observations.

1 Introduction

Coastal and marginal seas respond to climate forcing faster than the open ocean, whether the forcing arrives from the atmosphere, from land, or across lateral boundaries (Holt et al., 2025; Richardson et al., 2025; Wagawa and Igeta, 2025). The Mediterranean Sea is the archetype, changing at rates above the global ocean mean (Schroeder et al., 2017; Juza et al., 2022),

and within it the Adriatic Sea is a particularly sensitive sub-basin: semi-enclosed, 800 km long, 200 km wide and up to 1230 m deep, strongly influenced by riverine input, and subject to orographically shaped air–sea forcing.

Several Adriatic processes are directly relevant here. North Adriatic Dense Water forms on the shallow northern shelf and cascades along the bottom into the Jabuka and Southern Adriatic Pits, bringing oxygen to the deep layers (Zore-Armanda, 1963; Marini et al., 2006; Vilibić et al., 2023). The inflow of saline Levantine and Cretan Intermediate Water (LIW/CIW) is modulated on decadal scales by the Adriatic–Ionian Bimodal Oscillating System (Gačić et al., 2010; Civitarese et al., 2023), shaping the thermohaline properties and the nutrient budget of the basin (Civitarese et al., 2010). The Eastern Mediterranean Transient of the early 1990s, when the Aegean replaced the Adriatic as the dominant source of eastern Mediterranean deep water (Roether et al., 1996), is the precedent for an abrupt reorganisation on this scale, and it altered Adriatic properties directly (Vilibić et al., 2012). Open-ocean convection in the Southern Adriatic Pit supplies deep water to the Eastern Mediterranean (Gačić et al., 2002; Schlitzer et al., 1991). The small internal Rossby radius of the Adriatic makes its dynamics fast and spatially fine-grained (Cushman-Roisin and Korotenko, 2007; Pranić et al., 2023).

Since the early 2010s these processes appear to have moved outside their historical envelope. Salinity rose sharply after 2017 (Mihanović et al., 2021; Beg Paklar et al., 2020), dense waters formed in 2017, 2018 and 2022 were produced by weak cooling of very saline water rather than by strong cooling (Terzić et al., 2025a; Amorim et al., 2024; Le Meur et al., 2025), and near-surface salinity maxima were documented for the first time (Mihanović et al., 2021; Terzić et al., 2025b). Whether these are genuinely abrupt departures, or the visible part of a gradual trend sampled by a rapidly improving observing system, has not been tested formally. That distinction is important because the observing system changed at almost exactly the time the signal appeared: Argo entered the Adriatic in 2010 and now dominates the deep observations (Tintoré et al., 2019).

Three developments make a quantitative reassessment timely. The Adriatic in situ record has been consolidated across archives, so historical shipborne casts and modern autonomous profiles can be processed through a single pipeline. Argo now provides more than a decade of deep profiling in the Southern Adriatic Pit, enough to resolve the vertical structure of the change rather than only its surface expression. The same pipeline can also be applied to every Mediterranean sub-basin, which turns the recurring claim of local amplification from a qualitative impression into a testable ratio.

This research article is organised as follows. Section 2 describes the observational dataset and the methods. Section 3 addresses four questions: how large are the Adriatic changes, and are they distinguishable from sampling variability (Sects. 3.1–3.2)? Is the amplification relative to the Mediterranean general, or confined to particular depths (Sect. 3.3)? Did the vertical distribution of salinity in the intermediate layer change over time (Sect. 3.4)? Is the increase in near-surface salinity maxima (surface saline lakes) an abrupt shift or an artefact of vertical resolution (Sect. 3.5)? Sections 3.6–3.7 quantify the steric and double-diffusive consequences. Section 4 discusses the implications as hypotheses and identifies the observations and model experiments that would test them.

2 Data and methods

The analyses make three kinds of demand on the data, and the methods are organised accordingly. The climatological comparison (Sects. 2.1–2.3; Figs. 1 and 2) pools casts by region, period, season and depth so that two periods can be contrasted level by level, and needs an uncertainty estimate that allows for casts taken on the same cruise not being independent; the rate comparison with the rest of the Mediterranean (Sect. 2.4) fits trends to the same casts arranged as monthly series. The two feature detections – surface saline lakes (Sects. 2.5–2.6) and the intermediate salinity maxima (Sect. 2.7) – work on individual profiles rather than on the climatologies, so their main requirement is vertical resolution: a feature a few metres thick cannot be found in a cast sampled every ten metres, and both detections are therefore checked against the resolution of the record. The steric and double-diffusive analyses (Sects. 2.8–2.9) need the thermodynamic coefficients resolved through the full water column and use Argo profiles alone. Figure 3 shows the two detection criteria on measured profiles.

2.1 Observational dataset

Climatologies are built from the quality-controlled in situ temperature and salinity casts available in the Adriatic for 1950–1999 and 2000–2025, after the coastal and river-mouth exclusion of Terzić and Vilibić (2026c). Three archives are combined. The SeaDataNet Pan-European infrastructure supplies the Mediterranean aggregated dataset SDC_MED_DATA_TS_V2 (Simoncelli et al., 2020), which archives observations from 1911 to 2019, retrieved in December 2025. Local Adriatic databases are contributed by the Institute of Oceanography and Fisheries (IOR; Adriatic database 1987–2019) and the Ruđer Bošković Institute (RBI; northern Adriatic transect 1979–2017), together with the conductivity–temperature–depth (CTD) casts of the Croatian national monitoring programme under the Marine Strategy Framework Directive (MSFD, 2019–2023). The data collected in the Croatian Adriatic between 1952 and 1983 are published by Buljan and Zore-Armanda (1966, 1979) and Zore-Armanda et al. (1991). Argo profiles were retrieved in January 2026 through `argopy` (Maze and Balem, 2020) from the Argo Global Data Assembly Centre; the first Adriatic profile of the set dates from February 2010. The Adriatic casts used here are the Adriatic subset of the Mediterranean-wide multiplatform dataset assembled and described by Terzić and Vilibić (2026c), processed through the same chain, so the Adriatic and Mediterranean sides of the comparison in Sect. 2.4 rest on one dataset rather than on two independently curated ones. The cleaned Adriatic in situ files are archived on Zenodo by Terzić and Vilibić (2026a) (https://doi.org/10.5281/zenodo.20345373), the Mediterranean-wide processing pipeline by Terzić and Vilibić (2026b) (https://doi.org/10.5281/zenodo.20410481) and the analysis code specific to this paper by Terzić and Vilibić (2026d) (https://doi.org/10.5281/zenodo.23016822).

Table 1 reports retained cast counts by source, region, period, season and maximum depth. These are the counts entering Figs. 1–2, not the raw archive totals. Quality control follows the originating infrastructure: SeaDataNet procedures (SeaDataNet, 2010) and Argo real-time and delayed-mode procedures (Wong et al., 2023), with only flags 1 and 2 accepted in both. Casts from national and international cruises outside those archives were quality controlled following SeaDataNet procedures during the assessment described by Pranić et al. (2023). Within each source a cast is identified by its archive identifier, so no cast enters twice. The SeaDataNet aggregation also archives Argo float profiles as casts of its own; the 642 southern Adriatic

profiles of 2010–2019 that the Argo set holds as well are left out of every analysis, so that each profile is counted once. The aggregation further contains 1020 underway thermosalinograph records in the southern Adriatic, which are counted as casts and enter the 5 m bin only.

All analyses use the record to 2025. The climatological comparison (Figs. 1–2 and Table 1) contrasts 1950–1999 with 2000–2025, and the 33 664 casts of that table are drawn from those two windows.

The two periods are not sampled alike. Argo supplies 49.0 % of the 21st-century southern Adriatic casts and none of the 20th-century ones, and Argo profiles do not reach the top few metres – their median first sampled depth in the southern Adriatic is 5.5 m, against 3.1 m for the 21st-century casts of all platforms together – so the shallowest bins are the least comparable between periods (Sect. 3.1).

2.2 Regions, binning and climatologies

The northern and southern Adriatic are delimited by two polygons, labelled DJ1 and DJ3 after the Mediterranean sub-basin nomenclature of Manca et al. (2004). The labels follow that nomenclature but the boundaries do not: rather than straight lines of latitude, they follow the coastline and the bathymetry, so that the northern shelf is separated from the middle Adriatic along the Zadar–Ancona line and the southern Adriatic from the middle along the Gargano–Pelješac line. Bounding boxes are given in Table 1 and the polygon files are archived with the analysis code. Seasons are three-month bins, JFM, AMJ, JAS and OND. Casts are binned onto 22 standard levels between 5 and 1200 m. Argo profiles report pressure rather than depth; for the binning it is taken as depth, a difference of about 1 % that is small against the bin widths, whereas the profile-by-profile detection of Sect. 2.7 converts it to depth with the International Thermodynamic Equation of Seawater 2010 (TEOS-10) (IOC et al., 2010), so that floats and ship casts are read on one scale. A cast contributes to a level only where it carries a finite, flag-1 or flag-2 value; no vertical interpolation across gaps is performed, and casts that do not reach the full depth simply stop contributing below their deepest level. A level is retained when at least 5 % of the casts whose depth range spans it carry a valid value there. Each cast contributes one value per level, the mean of its measurements within the bin; the period mean is the average of these, and a second pass rejects cast values more than one standard deviation from the first-pass mean.

Temperature and salinity are binned as measured, that is as in situ temperature and practical salinity; practical salinity is a ratio and is therefore reported without units. Potential density anomaly referenced to the surface (σ_0) is derived from them through TEOS-10, which converts practical salinity to absolute salinity and in situ to conservative temperature internally, using the `gsw` implementation. The Argo-based analyses of Sects. 2.8 and 2.9 work directly in absolute salinity and conservative temperature, since they require the thermodynamic coefficients. The binning and pooling procedure is described in more detail by Terzić and Vilibić (2026c), who apply it Mediterranean-wide.

2.3 Uncertainty of climatological differences

Counting casts as independent measurements would overstate how much information the climatologies contain. A research cruise typically occupies a region for a few days and takes many casts in that time, so those casts largely repeat one synoptic

state rather than sampling the climate independently: 200 casts from four cruises carry far less information than 200 casts taken on 200 separate occasions.

The uncertainty is therefore computed with all casts of one data source taken on one day counted as a single independent observation; the day stands in for the cruise, which the cast index does not record. In practice, the variance of each period mean at each level is multiplied by the mean number of casts per such cruise-day in that region, period and season. This factor, the variance inflation factor, is at least one, so clustering always widens the interval: a value of 6 means the casts carry the information of about one sixth as many independent observations. For 2000–2025 it is 1.9–2.4 in the southern Adriatic and 5.5–6.2 in the northern Adriatic (for 1950–1999, when sampling was still more cruise-bound, 3.6–5.7 and 6.7–7.6, respectively), so the northern shelf, where cruises are denser and more repetitive, is far more strongly clustered. The 95 % confidence intervals on the differences between the periods follow from these inflated variances. The density differences of Figs. 1–2 are those of the potential density computed from the period means of temperature and salinity at each level. Potential density is a non-linear function of temperature and salinity, so its interval is obtained by recomputing it for 20 000 random combinations of the two drawn within their uncertainties. Shaded envelopes in the difference rows of Figs. 1–2 are these intervals; those in the period rows are ± 1 standard deviation of the observations contributing to each level.

Northern Adriatic results are reported only to 50 m, because below that depth the region is barely sampled: only 905 of the 13 602 casts of 2000–2025 reach 50 m or deeper, over 90 % of those stop between 50 and 75 m, and only 12 reach 100 m, against 2 in 1950–1999 (Table 1), so the 50–200 m column of that table describes a layer that in practice spans only 50–75 m.

2.4 Adriatic–Mediterranean rate comparison

Adriatic rates of change are compared with those of the rest of the Mediterranean. Deseasoned linear trends per decade are computed for each of the 28 Mediterranean sub-basins used by Terzić and Vilibić (2026c), labelled after Manca et al. (2004) (Sect. 2.2), three of which (DJ1–DJ3) are Adriatic. All 28 are processed with the same pipeline, bins, quality control and estimator, so that the Adriatic and Mediterranean rates are directly comparable. The monthly basin-by-depth series are built as by Terzić and Vilibić (2026c) and deseasoned with annual and semi-annual harmonics fitted to the whole 1950–2025 series; a linear trend is then fitted to the deseasoned values of 2000–2025 and is reported only where a series holds at least 36 monthly values and the window at least 24, a stricter floor than the 12 monthly values Terzić and Vilibić (2026c) require for their period-wise trends. Mediterranean values are the median, with the interquartile range, over the depth bins of a layer in the 25 sub-basins outside the Adriatic; Adriatic values are the median over the depth bins of the layer. The Adriatic sub-basins are excluded from the reference median so that the basin is not compared partly against itself; including them changes no ratio qualitatively (the largest effect is on surface salinity, 4.3 to 3.6). The four layers of Table 2 (5–50, 75–200, 250–600 and 700–1200 m) separate the seasonally mixed surface layer, the layer between the seasonal thermocline and the LIW/CIW horizon, the intermediate-water core, and the deep layers renewed episodically by cascading. The deep-layer result does not depend on these boundaries: the temperature ratio exceeds three at every level from 700 to 1200 m. The time window, 2000–2025, matches the climatologies; the resulting sampling asymmetry is quantified in Sect. 2.1.

To test how far the ratios depend on the cast population, the trends are also computed in every sub-basin from casts taken over water deeper than 800 m only, with the bottom depth at each cast taken from the GEBCO 2024 grid (GEBCO Compilation Group, 2024); series that hold fewer than 12 monthly values before 2010 are left out of this test, so that every open-water trend is fitted over the whole 2000–2025 window and not only over the years from 2010, when Argo makes open-water sampling dense. The 95 % intervals on the layer ratios come from resampling whole calendar years, the same years in every sub-basin (40 000 replicates). Depth thresholds of 500 and 1000 m, and floors of 0 to 36 monthly values, change the two upper-layer temperature ratios by 0.04 at most; the near-surface salinity ratio is more sensitive to the floor (Sect. 3.3).

2.5 Change-point analysis

Whether the change in the occurrence of surface saline lakes (SSLs) is a step rather than a gradual drift is tested on the casts themselves. The occurrence of an SSL in a cast is modelled as a logistic function of three things: a step at a break year, the season of the cast, and the platform (Argo float or ship cast). The break year is the one at which the model fits the casts best, and every year whose fit lies within the usual 95 % likelihood margin of that best fit is reported with it, as the set of years the data cannot tell apart. Because the feature occurs in the warm half of the year (Sect. 3.5), the test is run on the June–October casts, and repeated on all casts, on the summer casts alone, and within the ship casts and the Argo profiles separately.

Its p-value comes from a permutation that keeps the casts of each year together: whole years are reassigned to new positions in time, the best break is searched for again, and the fraction of 1000 such rearrangements that produce a step at least as large as the observed one is reported. The search for the break year is thus part of what is tested.

The test is made on the casts rather than on a series of annual occurrence rates, so that a year counts by its casts rather than as one vote, the season of each cast is allowed for, and the arrival of Argo floats in 2010, which by itself raises the detection rate (Sect. 3.5), enters as a term of its own rather than as part of the break.

Detection of an SSL depends strongly on vertical resolution (Sect. 3.5), so the test is run on a resolution-matched subset: casts with median level spacing ≤ 5 m and at least 8 levels in 0–100 m. The justification is a direct degradation experiment, in which Argo profiles are re-sampled onto progressively coarser grids and the identical detection is repeated (Fig. A1).

2.6 Detection of surface saline lakes

Detection uses raw profiles rather than the binned climatologies of Sect. 2.2, so the cast set is assembled separately and is larger: 9663 southern Adriatic casts over 1950–2025. Occurrence is shown from 1985 because nothing earlier can be evaluated: of the 313 casts from 1950–1984 whose vertical resolution can be computed, not one meets the resolution criteria of Sect. 2.5. Before 1975 no cast reaches even 10 m median spacing, let alone the 5 m required; the 1975–1979 casts are finer (68 % at 10 m, 12 % at 5 m), but those at 5 m carry only three or four levels in the upper 100 m against the eight the detection requires, and none combines the spacing with the level count (Fig. A1).

Following Terzić et al. (2025b), a cast is recorded as an SSL when all four of the following hold (Fig. 3a), with salinity throughout taken as practical salinity and its gradient therefore in m^{-1}: (i) the vertical salinity gradient falls below $-0.01\ \mathrm{m}^{-1}$ somewhere in 0–100 m, defining a halocline core, chosen among candidates as the one nearest 100 m; (ii) the maximum

salinity gradient above the core stays below $0.02\,\mathrm{m}^{-1}$, so the feature is not simply the lower flank of a shallower feature; (iii) the surface is at least 0.05 saltier than the core; and (iv) the water column above the core is statically stable in density, verified with a stratification index computed across the halocline with a 5 m vertical offset, so the salinity inversion is temperature-compensated rather than convectively unstable. Casts with fewer than 8 finite levels in the 0–100 m window, or without a usable temperature, are not evaluated. Occurrence among resolution-matched casts is shown in Fig. 4.

2.7 Detection of double salinity maxima

A southern Adriatic salinity profile can carry one subsurface salinity maximum or two, one above the other. Rather than tracking the depth of a single core, we locate every maximum in each cast, so that a cast with two maxima is described by two and any change in their separation can be measured.

A maximum is a level saltier than the levels above and below it. Most such levels are small ripples, so each is graded by its prominence: the drop in salinity from the maximum to the lowest value that must be crossed to reach a higher maximum in the same profile (Fig. 3b). A maximum is retained when its prominence is at least 0.010, ten times the precision of the archived values. Archived salinities carry three decimals, so the flat crest of a salty layer often shows two or more equal maxima separated by a dent of a few thousandths. These are one maximum, not several, so neighbouring maxima are counted as one unless the salinity dips by at least 0.010 between them, the saltier of them being kept. The threshold is a choice, and the detection is repeated for 0.005–0.030 in Appendix A.

Maxima are searched for between 20 and 900 m, with Argo pressures converted to depth (Sect. 2.2). The upper 20 m are excluded so that the near-surface maximum of a surface saline lake is not counted as an intermediate maximum. A cast must also carry at least 8 levels in the search range; this sets aside 479 of the 5069 SeaDataNet and Argo casts from 1950–2025 that carry both temperature and salinity (9.4 %) as too coarse; the IOR and MSFD casts of Table 1 do not enter this detection. Frequency statistics use only casts reaching 700 m, the depth to which the deep maximum descended in 2015–2016 (Mihanović et al., 2021). Those casts date from 1972–1998, 88 % of them from 1990–1998, and from 2010–2025, 99 % of them Argo profiles. In SeaDataNet the casts of 1999–2009 that reach 700 m are bathythermographs without salinity or belong to two CTD surveys whose temperature is flagged bad, and the IOR database holds only 16 casts of 2000–2009 that reach 700 m with both variables, too few for a period of their own; the two populations are therefore ship casts of the 1970s to 1990s and float profiles of 2010–2025.

Within each cast only the two most prominent maxima are kept, because a few very finely resolved historical profiles carry instrumental noise that the peak search reads as up to 266 maxima in one cast: 15 expendable-CTD casts of one cruise in May 1995 return 162–266 each and would, without the cap, supply 59 % of all 1950–1999 detections among casts reaching 700 m. The cap falls on both periods alike: 38.8 % of those casts in 1950–1999 and 39.2 % in 2000–2025 carry more than two maxima.

Each maximum carries its depth, salinity, temperature and σ_0; the density distinguishes a maximum displaced along its isopycnal from one made of different water. Detection runs at native vertical resolution and, because vertical sampling differs between the two samples (a quarter of the 1950–1999 casts reaching 700 m are bottle casts at 25 m spacing or coarser and most of the rest 1 m CTD profiles, whereas the floats sample every 2 m from 2019 on and every 10 m in most earlier profiles), is

repeated with every profile re-sampled to the historical standard depths (20, 30, 40, 50, 75, 100, 125, 150, 200, 250, 300, 400, 500, 600, 700, 800 and 900 m); both results are reported in Sect. 3.4. The periods are 1950–1999 and 2000–2025, as for the climatologies. Medians carry 95 % confidence intervals from resampling whole cruise-days (3000 replicates; for floats, whose successive profiles are days apart, each profile is a unit), distributions are compared between periods with a two-sided Mann–Whitney test, and the share of casts carrying two maxima with a chi-square test, which asks whether two proportions differ by more than their sample sizes allow. The exclusion depth, the prominence threshold (0.005–0.030), the number of maxima kept, the depth a cast must reach and the treatment of crest noise are all free choices, so the analysis is repeated with each of them varied in turn in Appendix A.

2.8 Steric decomposition

Thermosteric and halosteric height are computed from ascending Argo profiles reaching at least 1000 dbar in the Southern Adriatic Pit, following Wang et al. (2017), as

$$\mathrm{TSLA} = \int \alpha\,\Theta'\,\mathrm{d}z, \qquad \mathrm{HSLA} = -\int \beta\,S'_{\mathrm{A}}\,\mathrm{d}z, \tag{1}$$

where primes denote anomalies about the period-mean profile and α, β are the TEOS-10 thermal expansion and haline contraction coefficients. The integrand must be the anomaly Θ' rather than Θ itself: integrating $\alpha\Theta$ instead of $\alpha\Theta'$ makes the result, and its trend, depend on the temperature scale used, because Θ is measured from an arbitrary origin while α varies with depth. Anomalies remove that origin.

Profiles are interpolated onto a common 0–1000 dbar grid at 5 dbar spacing, the shallowest observation being carried to the surface since Argo does not sample the top few metres (median first sampled pressure 5.8 dbar for the profiles used here). Monthly means are formed and the annual and semi-annual harmonics removed, and trends are least-squares fits (Table 3).

Two features of the series govern how it is treated. First, successive months are correlated, so the window on which the trends are fitted, January 2014 to June 2024 (hereafter 2014–2024; Sect. 3.6), carries less information than its 116 monthly values suggest; the confidence intervals therefore rest on an effective sample size computed from the lag-one correlation of the residuals (Bretherton et al., 1999) (Fig. A2). For the 0–1000 m series that correlation is 0.7–0.8, leaving an effective 10–21 independent values, so the intervals are correspondingly wide. Second, the thermosteric and halosteric components move in opposition, and much of what makes each uncertain affects both in the same way and cancels in their sum. Adding two separately fitted trends would discard that cancellation and inflate the uncertainty on the net, so the net is formed profile by profile and trended once. Eighteen floats contribute 757 profiles from April 2010 to December 2025; WMO identifiers are listed in Table 4. Two further floats, 6903805 and 6901865, are excluded because only 6 of 33 and 1 of 78 of their profiles reach 1000 dbar.

2.9 Double-diffusive diagnostics

Two quantities are distinguished. The Turner angle determines whether the water column is in the salt-finger regime ($45^\circ \le \mathrm{Tu} < 90^\circ$); the density ratio R_ρ determines whether fingering there is dynamically effective. They are computed from vertical

gradients of conservative temperature and absolute salinity on the 5 dbar grid of Sect. 2.8 as

$$\mathrm{Tu} = \arctan \frac{\alpha\,\partial_z\Theta + \beta\,\partial_z S_\mathrm{A}}{\alpha\,\partial_z\Theta - \beta\,\partial_z S_\mathrm{A}}, \qquad R_\rho = \frac{\alpha\,\partial_z\Theta}{\beta\,\partial_z S_\mathrm{A}}, \tag{2}$$

with the four-quadrant arctangent, alongside the squared buoyancy frequency $N^2 = -(g/\rho)\,\partial\rho/\partial z$, which measures how strongly the water column is stratified. All are evaluated with the `gsw` implementation of TEOS-10 (IOC et al., 2010). Fingers transport salt appreciably for $R_\rho < 2$, marginally to about 4, and negligibly beyond about 10 (Schmitt, 1994): their growth time is set by R_ρ (Kunze, 1987), and they transport salt only if they reach full amplitude before internal-wave shear disrupts them. A water column can therefore be entirely finger-favourable by the Turner angle and still transport nothing, so two statistics are reported separately for each layer: the extent of the regime, the fraction of levels in the salt-finger regime, and its vigour, the fraction of those levels with $R_\rho < 2$. Both use the same 757 Argo profiles as the steric decomposition (Sect. 2.8) and, like it, need vertical gradients through the full column, repeated through the year; only Argo provides that here, so neither can be extended into the shipborne record.

Both quantities are evaluated separately in three depth layers, because their changes differ between layers and partly cancel when averaged over the whole column. The layers are 200–400 m, the classical range of the LIW salinity maximum (Artegiani et al., 1997); 400–600 m, immediately below it; and 600–1000 m, the deep layer. A fourth layer, 350–550 m, is computed only for comparison with the EMSO-E2M3A mooring record in Sect. 4.2. Profiles taken before 2017 are compared with those taken from 2017 onward with a two-sided Mann–Whitney test on the per-profile layer statistics; the same test is repeated on annual means, and the statistics are also computed with gradients taken over 25 dbar, because the floats report more levels in the later years (Sect. 3.7).

3 Results

3.1 Southern Adriatic warming and salinification

Between the 1950–1999 and 2000–2025 climatologies the southern Adriatic (DJ3) is warmer and saltier at every depth from 5 to 1200 m and in every season (Fig. 1), except near the surface in summer and autumn, as discussed below. Salinity differences range from $+0.108$ to $+0.531$ and are distinguishable from sampling variability at all 88 depth–season combinations after cruise-day clustering is accounted for. Temperature differences range from -1.27 to $+1.63\,^\circ$C, and 83 of the 88 are positive and significant (94 %). The summer of 1950–1999 is the sparsest season–period combination, 444 casts against 1708 in 2000–2025 (Table 1), so the summer temperature differences carry the widest intervals at most levels and are the ones most exposed to the sampling change discussed next.

The most negative of those differences, $-1.27\,^\circ$C in the 5 m summer bin, is an artefact of how the surface is sampled rather than a cooling. In summer 1950–1999, 82 % of southern Adriatic casts began at or above 1 m and the median first sample was at the surface; over 2000–2025 only 14 % do, the median first sample is at 2.5 m, and the Argo profiles first sample at a median 5.8 m. Binning does not remove this bias, because recent casts enter the shallowest bin only through its deeper, colder part: against the 20th-century summer gradient of $0.34\,^\circ\mathrm{C\,m^{-1}}$ between the 5 and 20 m levels, a sample at 2.5 or 5.8 m

instead of the surface reads colder by half a degree or more. A second sampling difference acts on the same levels: the summer casts are unevenly spread within the season. Of the 1950–1999 casts in the 5 m bin, 53 % were taken in August and 18 % in September; of the 2000–2025 ones, 18 % in August and 63 % in September. With the month mix of 1950–1999 the modern 5 m bin would be 0.9 °C warmer and the 10 m bin 0.3 °C warmer. The 5 m summer bin is therefore omitted from the difference row of Fig. 1. The 10 m summer difference, -0.44 °C, is also negative, and the 20 m one, -0.17 °C, is not distinguishable from zero. The summer differences above 30 m are therefore not interpreted, and neither are the two autumn differences that are not distinguishable from zero, -0.12 °C at 5 m and $+0.19$ °C at 10 m. Below 30 m, where the profile is smooth and the platforms overlap, the differences are positive at every level and season. Below 200 m the warming is 0.5–0.9 °C in every season (Fig. 1, bottom row).

Potential density has a weaker signal than either temperature or salinity: 57 % of depth–season combinations show a significant difference, because thermal and haline effects oppose one another. Below 600 m they largely compensate, the residual being within about 0.05 kg m^{-3}. This compensation is the physical statement behind the near-zero deep steric trend in Sect. 3.6.

3.2 Northern Adriatic shelf

In the northern Adriatic (DJ1, Fig. 2, 0–50 m) the pooled warming reaches 3.0 °C at 20 m in summer, and surface salinity is higher in every season, by $+0.09$ to $+0.18$ in winter, spring and autumn, the spring value not distinguishable from zero, but by $+1.00$ in summer, so the seasonal contrast between the fresh summer surface and the winter state is much reduced (Fig. 2). The evidence is weaker than in the south, and unevenly so: once clustering is accounted for, 79 % of the depth–season combinations reported here show a significant warming and 58 % a significant salinity increase; autumn is significantly cooler at 5 and 10 m, and salinity significantly lower at 10–20 m in spring and at 20 m in autumn. The northern shelf is where the clustering correction is largest, with variance inflation factors of 5.5–6.2 for 2000–2025, largely because one station at 13.7°E, 45.7°N, sampled several times a day in 1999–2004, supplies 54 % of the 2000–2025 northern casts, so that consecutive casts share one synoptic state (Sect. 2.3). The shelf is also where 20th-century sampling is concentrated along the western coastline, while salinity is systematically higher along the eastern one (Artegiani et al., 1997; Vilibić et al., 2019). The 21st-century casts sit farther east than the 20th-century ones (median cast longitude 13.7°E against 13.1°E), on the saltier side of that gradient, so the spatial sampling shift inflates rather than damps the apparent salinification. Northern Adriatic salinity differences should therefore be read as indicative upper bounds rather than established values, the temperature differences with the same caution, and we do not report DJ1 below 50 m at all (Sect. 2.3).

3.3 The amplification is depth-dependent

On matched periods and an identical pipeline (Table 2), the ratio of the southern Adriatic warming rate to the Mediterranean median is 0.55 at 5–50 m, 0.72 at 75–200 m, 1.5 at 250–600 m and 6.2 at 700–1200 m. Level by level it is close to one at 250–300 m and rises steadily with depth, exceeding six from 1000 m down. Thermal amplification is thus absent above 200 m and grows with depth below about 300 m.

However, the two ratios above 200 m should not be read as slower warming, for two reasons. First, they are medians over depth bins that differ: at 5 and 10 m the southern Adriatic warms at 0.43 and 0.57 °C per decade against a Mediterranean median of 0.44–0.45, whereas at 30–100 m it warms at 0.11–0.19 against 0.36–0.39 °C per decade. Second, most of the difference at 30–100 m reflects where the casts were taken. Casts over water deeper than 800 m make up about 40 % of a monthly mean until 2014 and about 75 % from 2015, as Argo floats in the open basin replace ship casts, and at 30–100 m the open basin is on average 0.4–0.7 °C colder than the shelf in the same month. With only such open-water casts used in every sub-basin (Sect. 2.4), the southern Adriatic rate at 30–100 m rises to 0.29–0.31 °C per decade, the Mediterranean median changes by 0.03 at most, and the layer ratios become 0.79 at 5–50 m and 0.86 at 75–200 m (95 % intervals 0.48–1.5 and 0.62–1.2), neither distinguishable from one. The test removes the change of location but not that of instrument: the southern Adriatic open-water casts are almost all bathythermographs until 2009 and floats from 2010. Whether the upper layers warm more slowly than the Mediterranean median therefore cannot be established. From 250 m down the ratios do not depend on the cast population (1.5 and 6.0 on open-water casts).

Salinity behaves differently. The salinity ratio is 4.3 at 5–50 m, 1.3 at 75–200 m, 1.9 at 250–600 m and 3.7 at 700–1200 m, so haline amplification is present through the whole column, with a minimum at 75–200 m, where the pooled ratio is not distinguishable from one (95 % interval 0.88–2.5) but the open-water ratio is 2.1 (1.2–3.4). The near-surface ratio also depends on the cast population, because the open basin is 0.2–0.8 saltier than the shelf in the upper 40 m: on open-water casts the southern Adriatic salinification rate falls from 0.22 to 0.16 per decade and the ratio to 3.4 (1.3–18). The southern Adriatic is therefore salinifying faster than the Mediterranean median through the column, but warming faster than it only below about 300 m. These ratios compare mean rates over the window and say nothing about acceleration, which Terzić and Vilibić (2026c) find to peak in the Adriatic–Ionian sector.

3.4 The intermediate salinity maximum has lost its dominant band

The classical description of the southern Adriatic intermediate layer is of a single salinity maximum, associated with the inflow of Levantine Intermediate Water and typically found between 200 and 400 m (Artegiani et al., 1997). We test that description directly by detecting every prominent salinity maximum in each cast rather than one core depth (Sect. 2.7), and asking where those maxima sit.

The change is in where the maxima lie rather than in how many there are. Two maxima are not a modern feature: among casts deep enough to resolve both, 59.9 % carried two in 1950–1999 and 62.6 % in 2000–2025 ($p = 0.24$, chi-square). The share depends on the detection settings: across the settings of Sect. 2.7 it rises significantly in two configurations and falls significantly in one (Fig. A3c), so no trend in it is claimed. What did change is their concentration. In 1950–1999 the detections cluster in one band: 27 % of them fall in a single 50 m interval at 100–150 m and 41 % within 100–200 m. This band is not a definition of the core but simply the interval in which the historical detections cluster; it lies immediately above the classical 200–400 m range. In 2000–2025 that same band holds only 16 %, and the detections spread through the column in both directions: 47 % now lie above 100 m against 29 % before, and 27 % at or below 300 m against 16 %, with a second mode at

400–600 m (Fig. 5). The historical profile therefore had a dominant intermediate maximum, which a single-core description represents adequately; the modern one does not.

The two maxima have also moved apart. In casts that carry both, the vertical distance between them has a median of 122 m in 1950–1999 and 210 m in 2000–2025 ($p = 10^{-10}$, Mann–Whitney), and its spread grew from an interquartile range of 72–206 m to 60–412 m. Pooled over the same casts, the upper maximum sits at a median depth of 82 m (95 % confidence interval 75–91 m) in 1950–1999 and 64 m (62–67 m) in 2000–2025, and the lower one at 205 m (185–230 m) and 333 m (312–364 m); the intervals do not overlap for either. The difference between these pooled medians need not equal the median within-cast distance: the pooled medians describe where each maximum typically lies, the within-cast distance how far apart the two are in a typical cast. The two maxima also diverged in density: the upper one became 0.13 kg m^{-3} lighter as it salinified, while the lower one changed by only 0.03 kg m^{-3} and so stayed close to its isopycnal. Water that is at once saltier and markedly lighter must be warmer, so it cannot be the same water pushed upward: the two maxima are not one migrating core.

They have not, however, become sharper. The salinity drop from the weaker maximum to the minimum between the two, which measures how distinctly the pair stands apart, is unchanged: a median of 0.030 in 1950–1999 and 0.026 in 2000–2025, with overlapping confidence intervals (0.024–0.037 and 0.025–0.028). The maxima are therefore differently placed rather than better resolved.

Two checks support these results. Repeating the detection with every profile re-sampled to the historical standard depths gives 41.9 % of detections in the 100–200 m band for 1950–1999 and 20.0 % for 2000–2025, compared with 40.9 % and 15.7 % at native resolution, so the contrast is not an effect of the difference in vertical sampling. The concentration in that band is higher in 1950–1999 than in 2000–2025 under every detection setting and every treatment of profile noise we tested, as is the excess lightening of the shallow member over the deep one (Fig. A3).

3.5 Surface saline lakes: an abrupt shift

Detection rates differ by a factor of about 27 between the data sources of Table 1 in the full cast set of Sect. 2.6, before resolution matching: 0.56 % for SeaDataNet, 3.76 % for the IOR Adriatic database, 12.14 % for the Croatian MSFD monitoring casts and 14.87 % for Argo. The sources are archives rather than instrument types – the MSFD casts are ordinary CTD profiles – and they cover different years, so the spread mixes the effect of period with that of vertical resolution. The degradation experiment isolates the second (Fig. A1): re-sampling Argo profiles onto coarser grids leaves detections unchanged at 2 m (439 against 437 at native 1–5 m spacing) but reduces them to 237 at 5 m and 48 at 10 m, in profiles that demonstrably contain a surface saline lake, because the criterion requires a salinity gradient steeper than $-0.01\,\mathrm{m}^{-1}$ across a feature a few metres thick. On the standard bottle grid (0, 10, 20, 30, 50, 75, 100 m) no profile can be evaluated at all, since the grid carries seven levels in the upper 100 m against the eight the detection requires. The near-zero historical occurrence is therefore partly instrumental, and Fig. 4 is built on resolution-matched casts.

The resolution threshold retains 4749 of the 5673 casts for which a level spacing in 0–100 m could be computed. Enough historical data meets it: SeaDataNet holds substantial high-resolution CTD in the southern Adriatic, with a median level spacing of 1 m, so 81 of the 119 casts in 1985–1989 and 1211 of the 1570 casts in 1990–1999 satisfy the spacing and level-count criteria,

against 2128 of 2129 in 2016–2025. Among the matched casts the shipborne contribution of SeaDataNet all but ends in 2009 (16 casts in 2012–2015), so from 2010 the record rests on Argo (91 % of the matched casts), on the IOR database to 2019 (172 casts) and on the Croatian monitoring CTD from 2019 (96 casts).

On the June–October casts the change-point model of Sect. 2.5 places the step after 2014, and no other year comes within the 95 % margin of that fit. Occurrence rises from 4.9 % of casts before it to 38.4 % after ($p = 0.02$), an odds ratio of 9.4 (6.6–13.6). The step is not the arrival of Argo. Within the ship casts alone it falls after 2016 (the years 2006–2016 cannot be told apart) and takes occurrence from 3.7 to 32.5 % ($p = 0.014$); within the Argo profiles alone it falls after 2014 and takes it from 7.1 to 39.9 % ($p = 0.08$). Floats do detect more often than ships in the same year and season, by an odds ratio of 2.0 (1.4–2.9); on the casts the step falls after 2014 whether or not the platform is allowed for. The same holds when the season is varied: on all casts of the year, ship and float together, the break is again after 2014 and occurrence rises from 3.2 to 18.3 % ($p = 0.13$); on the summer casts alone, again ship and float together, it rises from 4.9 to 47.3 % ($p = 0.02$); and within each platform the seasonal subsets place the break between 2014 and 2016 as well.

The change is seasonal (Fig. 4B). Between 1950–1999 and 2000–2025, summer occurrence rises from 1.7 % (3 of 180 matched casts) to 34.4 % (303 of 880), and autumn from 3.8 % to 13.9 %, whereas winter occurrence stays at or below 1.3 % in both periods, indicating that winter mixing did not weaken comparably.

The pooled properties of the detected cores also differ between the periods (Fig. 4C–F): the median core sits at 19 m against 31 m, with a much stronger temperature gradient at the core (median -0.63 against $-0.20\,^{\circ}\mathrm{C\,m^{-1}}$) and density step, while the salinity gradient that defines the feature is unchanged. Most of that contrast, however, is the shift of the detections into summer, when cores are shallow and sharply capped: summer holds 63 % of the modern detections against 9 % of the historical ones.

The shift does not coincide with 2017: it falls after 2014, so occurrence stepped up in the middle of the decade, with 2017 the most extreme year (46 % of all matched casts) within an already elevated regime.

Resolution alone, however, does not explain the historical rarity. The 1211 casts from the 1990s that do meet the resolution criteria yield only 2.1 % detections, against 19.0 % in 2016–2025 on a comparable sample. The degradation experiment establishes only that the coarser part of the historical archive could not have detected these features at all, so absence from that part of the record is not evidence of absence from the ocean; the resolution-matched casts remain the ones that can size the increase, and they show the step.

3.6 Steric decomposition: the net contribution is negative

Thermosteric and halosteric height are decomposed separately from the Argo record over the 2014–2024 window of Sect. 2.8, the most recent decade with near-continuous float coverage (116 of 126 months). Over 0–1000 m (Table 3) the thermosteric trend is $+9.80 \pm 2.71$, the halosteric -15.21 ± 2.33 and the net $-5.41 \pm 2.49\,\mathrm{mm\,yr^{-1}}$ (Fig. A2): halosteric contraction dominates, and the steric term acts to lower local sea level rather than to raise it. The sign of the net depends on the window. On the whole Argo record, April 2010 to December 2025, the net is $-1.2\,\mathrm{mm\,yr^{-1}}$, on January 2012 to December 2025 -1.4 and on January 2014 to December 2025 $-2.2\,\mathrm{mm\,yr^{-1}}$: negative in the central estimate, but not distinguishable from zero. What holds on every window tested is the structure of the decomposition, a significantly positive thermosteric trend opposed by a

halosteric one of at least comparable size, while the significantly negative net is a property of the well-sampled 2014–2024 decade.

Integration depth explains most of the apparent disagreement with published Mediterranean values. Recomputed on the 0–400 m layer used by Mohamed and Skliris (2022), the thermosteric rate is $+2.26 \pm 1.37\,\mathrm{mm\,yr^{-1}}$ against their eastern Mediterranean mean of $+2.13 \pm 0.41$: the rates agree once the layers match, and three quarters of the southern Adriatic thermosteric signal lies below 400 m. The halosteric term does not converge (-6.81 ± 2.55 against -0.75 ± 0.19), and that difference is real rather than methodological – Adriatic salinification over 2014–2024 far exceeds the eastern Mediterranean mean over 1993–2019. In the 600–1000 m layer the thermosteric and halosteric trends are individually well determined, $+5.7 \pm 0.9$ and $-5.6 \pm 1.0\,\mathrm{mm\,yr^{-1}}$, and compensate almost exactly, leaving a net of $+0.1 \pm 0.5\,\mathrm{mm\,yr^{-1}}$ that is consistent with zero. The compensation itself, not the residual, is the result; it matches the deep density result of Sect. 3.1.

These are decadal rates from Argo floats alone over a window that spans the post-2017 episode, and they are not secular climate trends, since deep renewal is episodic (Fig. 6). For comparison with the longer record, the same quantities are also differenced between the two climatologies of Sect. 2.2 and expressed as a rate. The casts entering them cluster in the 1990s and the 2010s, with mean years 1993 and 2014, so the effective separation is 21 years, not 50. On that basis the thermosteric difference is $+7.4$ and the halosteric $-7.0\,\mathrm{mm\,yr^{-1}}$, with a net of $+0.4\,\mathrm{mm\,yr^{-1}}$ whose sign changes with the season and the data source. The halosteric term of 2014–2024 is about 2.2 times this climatological rate and the thermosteric term 1.3 times, so most of what distinguishes the recent decade is in the salt.

3.7 Salt fingering: the change is below the LIW core

The double-diffusive diagnostics behave differently above and below the base of the classical LIW core (Table 5, Fig. 7).

Within the core itself, over 200–400 m, neither the extent nor the vigour of the regime (Sect. 2.9) changes distinguishably from sampling variability: 55.3 % before 2017 against 56.0 % after ($p = 0.9$) for the extent, and 34.6 % against 32.3 % ($p = 0.17$) for the vigour. The only significant change within the core is a weakening of the stratification, the median N^2 falling by 16 %.

Below the core the picture changes. Over 400–600 m the finger-favourable fraction rises from 56.6 % to 60.3 % ($p = 0.03$) and the vigorous fraction from 28.0 % to 39.0 % ($p = 4 \times 10^{-9}$), while median N^2 falls by 56 %, from 2.50×10^{-6} to $1.10 \times 10^{-6}\,\mathrm{s^{-2}}$. That contrast depends on the split year: the layer was already vigorous in 2013–2014, with annual medians of 67 and 46 % (Fig. 7d), so a split at 2016 shows no change (36 against 35 %), whereas splits at any year from 2017 to 2020 all do. The deep-layer contrast below holds for every split year from 2016 to 2020 ($p < 10^{-47}$), and the core shows no change for any of them. In the deep layer, 600–1000 m, the regime was already close to saturation in extent before 2017, occupying 92.1 % of levels, and edges down to 87.7 % after; what changes there is vigour, and it changes more than anywhere else, from 10.7 % to 37.4 % ($p = 7 \times 10^{-81}$). The deep layer was thus finger-favourable in both periods, but only after 2017 did a large part of it reach the density ratios at which fingers transport salt.

This depth structure matches the one in Sect. 3.4. Between the 1950–1999 and 2000–2025 periods the deeper salinity maximum descended from a median 205 to 333 m, from the top of the classical core towards its lower part, and the share of

deeper maxima lying at 400 m or deeper rose from 16 to 43 % (34 % now lie at 400–600 m, against 11 % before). Fingering intensified in the layers into which a growing share of the deeper maxima has moved, and did not change in the core, where their share fell from 37 to 23 %.

The stratification weakened alongside: per profile, N^2 falls significantly in all three layers, by 16, 56 and 32 % at 200–400, 400–600 and 600–1000 m respectively.

The intensification does not coincide with 2017 (Fig. 7d). In the deep layer the median vigorous fraction per profile is below 1 % in 2010–2012, 8–10 % in 2013–2016, 14 % in 2017 and 28 % in 2020, jumps to 52–62 % in 2021–2023 and relaxes to 30 % in 2025. In the core the finger-favourable fraction, 60–83 % in 2017–2020, fell to 30 % in 2025, which is why its post-2017 mean is no higher than the pre-2017 one. In the 400–600 m layer the rise comes earlier, from 18 % in 2017 to 71 % in 2020, so that it reaches the layer below the core before the deep layer, which is the order a downward transfer of salt requires.

Two checks qualify these results. The tests of Table 5 treat profiles as independent; on annual means only the increase in vigour and the fall of N^2 in the deep layer remain significant (both $p = 0.0004$). And the floats report more levels in the later years (median spacing at 600–1000 m 24 dbar before 2017, 10 dbar from 2017); with gradients taken over 25 dbar throughout, the vigour still rises below the core and not within it. The contrast between the core and the layers below it therefore rests on vigour, and the firm result is the rise in vigour of the deep layer.

4 Discussion

4.1 A coupled advective and local mechanism

The results are consistent with remote and local mechanisms acting together, and with neither alone. Progressively warmer and saltier Eastern Mediterranean source water supplies an increasingly saline reservoir at the southern boundary (Skliris et al., 2025; Schroeder et al., 2017), while local preconditioning determines how and where that salt is redistributed within the basin: reduced river discharge lowers the Adriatic freshwater budget (Verri et al., 2024), and the exceptional salinities of 2017 and their basin-scale preconditioning are documented by Mihanović et al. (2021). We have no observational budget for evaporation or winter mixing. The seasonal breakdown of Sect. 3.5 places the preconditioning in the warm season, since summer and autumn surface-lake occurrence rose sharply while winter occurrence did not, so the change acts on the summer surface layer rather than on winter convection.

The salinity-maximum result constrains the mechanism further. The deeper maximum stayed near its isopycnal, which is what advection of a denser saline core into a warming basin would produce, while the shallower one became much lighter as it salinified, which requires a different and shallower source. These are two pathways rather than one migrating feature, and a single-core description cannot represent both. Mihanović et al. (2021) see the same split in the 2015–2017 episode, with new high-salinity water arriving nearer the surface from 2015 while the saline core deepened, though their excursion is far larger because they track individual floats through a particular sequence of years where we take medians over multi-decadal periods.

Reported LIW depths vary too much between regions to serve as a baseline for any of this. The intermediate salinity maximum lies at 200–500 m for the Mediterranean as a whole and at 300–800 m in the western basin (Schroeder and Chiggiato,

2022), while Argo places it at 200–600 m Mediterranean-wide (Kubin et al., 2019) and at about 100–250 m in the eastern Mediterranean over 2015–2017 (Fach et al., 2021). The 200–400 m of the classical southern Adriatic description (Artegiani et al., 1997), the range we test against and the one our layers follow, sits within that spread.

One hypothesis follows, which the present data are consistent with but do not establish: the depth-dependence of the amplification (Sect. 3.3) is the signature of this same split. Thermal amplification grows with depth because renewal of the deep layers is episodic, while the upper layers are ventilated fast enough by air–sea exchange not to exceed the Mediterranean median; haline amplification is present through the column because salt arrives both at the surface and at depth. That the same sector emerges as the locus of Mediterranean-wide acceleration (Terzić and Vilibić, 2026c) is consistent with this reading, as is the depth structure of the double-diffusive result.

4.2 Density, sea level and ventilation

The steric decomposition bears directly on local sea level. With a net steric contribution of $-5.4 \pm 2.5\,\mathrm{mm\,yr^{-1}}$ the steric term opposes rather than drives local sea level rise, so any observed rise in the Southern Adriatic must be mass-driven. This is consistent with Verri et al. (2024), who attribute the recent northern Adriatic sea level decline to a regional water deficit. It rests on a single Argo decade: the sign is robust over 2014–2024, but on windows extending to 2025 the net is not distinguishable from zero (Sect. 3.6), so whether it persists cannot be settled from this record.

Deep ventilation of the pit is episodic. From moorings over 2012–2022, Le Meur et al. (2025) identify gravity currents reaching the deep Southern Adriatic in only four years, 2012, 2017, 2018 and 2022; the first followed an exceptionally strong and prolonged bora outbreak that formed very cold, dense water (Mihanović et al., 2013). Deep properties therefore respond as a series of steps rather than as a gradual drift, each event resetting them before they relax again (Fig. 6), and the sign of the reset has changed: in the earlier regime (Querin et al., 2016) cascading water arrived cold and cooled the deep layer, whereas since 2017 it arrives only weakly cooled but much saltier and leaves the layer warmer and saltier than it found it (Terzić et al., 2025a). The deep trends of Sect. 3.6 are individually significant, but this saw-tooth is why a decade cannot show whether they are secular. Saline water needs less cooling to sink, so the shift toward haline-driven formation could sustain ventilation under milder winters; but the water so formed is warmer and carries less oxygen (Ingrosso et al., 2017; Chiarini et al., 2022), so it could equally degrade it. Our data do not show which of the two prevails.

The double-diffusive result locates another mechanism, active in the recent decade. Salt fingering has intensified below the classical LIW core and not within it, in the layers into which a growing share of the deeper salinity maxima has moved (Sect. 3.7) and in which the stratification has weakened. It has become more effective in the layer where the salt now arrives, though there the contrast depends on the years compared (Sect. 3.7), and below it the deep layer, already close to saturation in extent, more than tripled the fraction in which fingers actually transport salt. Salt descending out of the core meets a column newly capable of carrying it further down, though we have not measured a flux.

Amorim et al. (2024) report the same transition from the EMSO-E2M3A mooring in this pit, finger-favourable conditions rising from 27 % to 72 % of observations across the winter of 2016/17. Their 350–550 m layer straddles the base of the core, where we also find the change; recomputed on it our diagnostics rise from 48.6 to 56.9 % in extent and 29.1 to 36.9 % in vigour

(Table 5). Both analyses find an increase there, in ours significant only when profiles are treated as independent (Sect. 3.7), which is as far as the agreement can be taken, since a mooring sampling one position continuously and a float array sampling the pit every few days do not measure the same quantity.

4.3 Biogeochemical and ecological implications

The following are plausible pathways, not effects quantified here, and we limit them to the changes reported above.

A near-surface salinity maximum has two competing effects on vertical exchange and our analysis resolves neither. It increases the density stability of the upper column, which acts to suppress exchange of oxygen, nutrients and carbon with the intermediate layers (Jacox and Edwards, 2011; Breitburg et al., 2018; Bourgeois et al., 2022), with consequences for production, microbial food webs and air–sea carbon exchange (Cantoni et al., 2024; Martellucci et al., 2025b). Elevated salinity also constrains growth directly through osmotic stress: the record salinities of 2017 coincided with markedly lower bacterial production and lower abundances of most picoplankton groups than in the preceding decade (Beg Paklar et al., 2020). But salinity decreasing with depth beneath the maximum is itself finger-favourable, so the same feature may instead promote downward transport. Our diagnostics begin at 200 m and cannot say which dominates in the surface layer; dedicated observations there are required.

Whether the redistribution of the intermediate maxima promotes or suppresses production likewise depends on the upstream history of the inflowing water, on whether its nutrients were drawn down in the euphotic zone before it entered the basin (Ozer et al., 2022; Reich et al., 2026), which our results do not resolve.

For ecosystems, documented impacts and projected vulnerabilities should be kept apart. Three effects have been observed in the Adriatic: mass mortality linked to warming (Kružić et al., 2016), mussel mortality in coastal waters (Capriotti et al., 2025), and redistribution of benthic species toward northern coastlines (Matić-Skoko et al., 2022; Bellin and Rossi, 2024). Others remain projections: that further redistribution will be constrained by the basin's semi-enclosed geometry and by the limited cold-water refugia of the middle Adriatic depressions (Chiarini et al., 2022; Carlot et al., 2025), with consequences for the fisheries that exploit them (Martinelli et al., 2023; Kamberi et al., 2025). For aquaculture, the relevant change is the bottom-water warming and salinification documented in Sect. 3.1 (Cetinić, 2024; Haberle et al., 2024).

4.4 Limitations

The climatological comparison rests on a changing observing system, and we have controlled for this where it is testable – by resolution matching for SSL detection, by degradation experiments for the salinity maxima, and by cruise-day clustering for the difference profiles – but not everywhere. Northern Adriatic salinity remains the weakest element, because 20th-century sampling is concentrated on the western side of a basin with a strong east–west salinity gradient. The Argo-based steric and double-diffusive results describe the Southern Adriatic Pit over 2014–2024 and 2010–2025 respectively, a decade to a decade and a half, which cannot separate a secular climate trend from the episodic cycle of deep renewal.

The larger gap is that this is an ocean-side analysis throughout: we establish when the changes occurred and how they are distributed in the vertical, but not what forced them. Wintertime turbulent heat flux anomalies over the northern Adriatic

formation region do not share a common cooling signature across the recent cascading years: 2018 and 2022 carry positive anomalies, that is weaker heat loss, relative to the 1980–2010 baseline, so the density required for cascading in those years cannot have come from heat loss alone (Terzić et al., 2025a). That is consistent with the mechanism proposed above, but the flux estimate is coarse: the reanalysis behind it underestimates the cooling along the bora jets (Denamiel et al., 2021), where much of the relevant heat loss occurs. Establishing how much of the change reported here follows from bora frequency, evaporation and river discharge requires a dedicated surface-flux and freshwater budget over the formation regions, resolved finely enough to capture the jets. Until that is done, the mechanism of Sect. 4.1 remains a hypothesis rather than an attribution.

5 Conclusions

Three findings are supported by the analyses presented here. **First, southern Adriatic salinification between 1950–1999 and 2000–2025 is significant at all 88 depth–season combinations, and warming at 94 % of them**, the exceptions being the five near-surface summer and autumn levels where the two periods are sampled differently (Sect. 3.1). The amplification relative to the Mediterranean, the ratio of the southern Adriatic rate to the median rate of the other Mediterranean sub-basins over 2000–2025 (Sect. 3.3), is depth-dependent: for temperature it is absent above 200 m and reaches 6.2-fold at 700–1200 m. Haline amplification is present through the whole column, 4.3-fold at the surface and 3.7-fold at 700–1200 m. **Second, the increase in near-surface salinity maxima is a genuine level shift after 2014, seen in ship and float records alike**, from 5 to 38 % of warm-season casts, and is demonstrable only once vertical resolution and platform are controlled for. The coarser part of the historical archive could not have detected these features at all, yet even among the historical casts that could, occurrence was far rarer: 2.1 % in the 1990s against 19.0 % in 2016–2025. **Third, the intermediate salinity maximum has lost its dominant band**: the share of detected maxima within 100–200 m falls from 41 % to 16 % between the periods, while the share of casts carrying two maxima is unchanged. Where two coexist they move apart, the deeper one descending from a median 205 to 333 m while remaining close to its isopycnal and the shallower one rising from 82 to 64 m; only the shallower one becomes markedly lighter as it salinifies, which points to a different and shallower source.

Two further results bear on the mechanism. **The steric contribution in the Southern Adriatic Pit over 2014–2024 is $-5.4 \pm 2.5\,\mathrm{mm\,yr^{-1}}$, negative rather than positive**, so local sea level rise over that decade must be mass-driven; on windows extending to 2025 the net is not distinguishable from zero. Moreover, **salt fingering has intensified below the classical intermediate core and not within it**, in vigour more than in extent and most firmly at 600–1000 m, alongside a weakening of stratification measurable in N^2; the layers into which a growing share of the deeper salinity maxima has descended are therefore also those newly capable of carrying salt further down.

The consequences for ventilation, biogeochemistry and ecosystems remain hypotheses. Testing them requires sustained in situ observing at a vertical resolution able to resolve the features described here, and high-resolution coupled physical–biogeochemical modelling able to represent episodic deep renewal. It would also be served by an update of the SeaDataNet Mediterranean aggregation, which currently ends in 2019 and holds no shipborne cast in the southern Adriatic after 2015:

the most recent six years of shipborne hydrography are precisely those in which the changes reported here developed, and at present only Argo and the Croatian monitoring casts cover them.

Code and data availability. The cleaned in situ data are archived on Zenodo by Terzić and Vilibić (2026a) (https://doi.org/10.5281/zenodo.20345373), the Mediterranean-wide processing pipeline by Terzić and Vilibić (2026b) (https://doi.org/10.5281/zenodo.20410481) and the analysis code and derived tables specific to this paper by Terzić and Vilibić (2026d) (https://doi.org/10.5281/zenodo.23016822). The SeaDataNet record ends in 2019; the 2020–2025 part of the 2000–2025 window is supplied by Argo and by the Croatian monitoring casts to 2023. The SeaDataNet Mediterranean aggregated dataset SDC_MED_DATA_TS_V2 is available from https://www.seadatanet.org; Argo data are freely available from the International Argo Program (https://argo.ucsd.edu) and were accessed through `argopy`. The Argo floats used in the Southern Adriatic Pit analyses (Sects. 2.8–2.9) are listed in Table 4. Floats 6903805 and 6901865 were excluded from the steric analysis because only 6 of 33 and 1 of 78 of their profiles reach 1000 dbar; all other ascending profiles reaching 1000 dbar were retained.

Author contributions. ET: conceptualisation, methodology, formal analysis, investigation, data curation, software, visualisation, writing – original draft, writing – review and editing. IV: conceptualisation, methodology, writing – original draft, writing – review and editing, funding acquisition.

Competing interests. The authors declare that they have no competing interests.

Acknowledgements. We are grateful to all researchers who developed the concepts and collected the observations on which this study rests. We acknowledge the provision of temperature and salinity data by the SeaDataNet Pan-European Infrastructure, the Institute of Oceanography and Fisheries, the Ruđer Bošković Institute, and Italian marine research institutions. The Argo data were collected and made freely available by the International Argo Program and the national programs that contribute to it (https://argo.ucsd.edu, https://www.ocean-ops.org); the Argo Program is part of the Global Ocean Observing System. We thank the two anonymous reviewers and the topical editor for their careful reading and for comments and suggestions that greatly improved the article. This research was supported by the Croatian Science Foundation through projects GLOMETS (IP-2022-10-3064) and C3PO (IP-2022-10-9139) and the incoming mobility scheme for postdoctoral researchers (MOBDOL-2023-12), the Interreg Italy–Croatia Programme 2021–2027 project AdriaClimPlus (ITHR0200333), and the EU NextGeneration project AdriaClimRisk (PK.3.4.17.0001).

References

Amorim, F. L. L., Le Meur, J., Wirth, A., and Cardin, V.: Tipping of the double-diffusive regime in the southern Adriatic Pit in 2017 in connection with record high-salinity values, Ocean Sci., 20, 463-474, https://doi.org/10.5194/os-20-463-2024, 2024.

Artegiani, A., Bregant, D., Paschini, E., Pinardi, N., Raicich, F., Russo, A.: The Adriatic Sea general circulation. Part I: Air–sea interactions and water mass structure. J. Phys. Oceanogr., 27, 1492–1514, https://doi.org/10.1175/1520-0485(1997)027<1492:TASGCP>2.0.CO;2, 1997.

Beg Paklar, G., Vilibić, I., Grbec, B., Matić, F., Mihanović, H., Džoić, T., et al.: Record-breaking salinities in the middle Adriatic during summer 2017 and concurrent changes in the microbial food web. Prog. Oceanogr., 185, 102345, https://doi.org/10.1016/j.pocean.2020.102345, 2020.

Bellin, N., Rossi, V.: Modeling the effects of climate change on the habitat suitability of Mediterranean gorgonians. Biodivers. Conserv., 33, 929–948, https://doi.org/10.1007/s10531-024-02779-z, 2024.

Bourgeois, T., Goris, N., Schwinger, J., Tjiputra, J. F.: Stratification constrains future heat and carbon uptake in the Southern Ocean between 30°S and 55°S. Nat. Commun., 13, 340, https://doi.org/10.1038/s41467-022-27979-5, 2022.

Breitburg, D., Levin, L. A., Oschlies, A., Grégoire, M., Chavez, F. P., Conley, D. J.: Declining oxygen in the global ocean and coastal waters. Science, 359, 6371, https://doi.org/10.1126/science.aam7240, 2018.

Bretherton, C. S., Widmann, M., Dymnikov, V. P., Wallace, J. M., and Bladé, I.: The effective number of spatial degrees of freedom of a time-varying field, J. Climate, 12, 1990-2009, https://doi.org/10.1175/1520-0442(1999)012<1990:TENOSD>2.0.CO;2, 1999.

Buljan, M. and Zore-Armanda, M.: Hydrographic data on the Adriatic Sea collected in the period from 1952 through 1964, Acta Adriat., 12, 1–438, 1966.

Buljan, M. and Zore-Armanda, M.: Hydrographic properties of the Adriatic Sea in the period from 1965 through 1970, Acta Adriat., 20, 1–368, 1979.

Cantoni, C., De Vittor, C., Faganeli, J., Giani, M., Kovač, N., Malej, A.: Carbonate system and acidification of the Adriatic Sea. Mar. Chem., 267, 104462, https://doi.org/10.1016/j.marchem.2024.104462, 2024.

Capriotti, M., Bracchetti, L., Cocci, P., Mazzocchi, V., Fazzini, M., Corvaro, F., et al.: In situ investigation of ecological and molecular stress mechanisms triggered by marine heat waves in Adriatic populations of the Mediterranean mussel. Diversity, 17, 385, https://doi.org/10.3390/d17060385, 2025.

Carlot, J., Galobart, C., Gómez-Gras, D., Santamaría, J., Golo, R., Siniet, M., et al.: Vulnerability of benthic trait diversity across the Mediterranean Sea following mass mortality events. Nat. Commun., 16, 1571, https://doi.org/10.1038/s41467-025-55949-0, 2025.

Cetinić, A. B.: Shellfisheries in Croatia: from manual collection to contemporary practices, Naše More, 71, 154-165, https://doi.org/10.17818/NM/2024/3.8, 2024.

Chiarini, M., Guicciardi, S., Zacchetti, L., Domenichetti, F., Canduci, G., Angelini, S., et al.: Short-term evaluation of changes in fisheries management measures in the Pomo/Jabuka Pits area. Sustainability, 14, 7742, https://doi.org/10.3390/su14137742, 2022.

Civitarese, G., Gačić, M., Lipizer, M., Borzelli, G. L. E.: On the impact of the BiOS on the Adriatic and Ionian Seas. Biogeosciences, 7, 3987–3997, https://doi.org/10.5194/bg-7-3987-2010, 2010.

Civitarese, G., Gačić, M., Batistić, M., et al.: The BiOS mechanism: History, theory, implications. Prog. Oceanogr., 216, 103056, https://doi.org/10.1016/j.pocean.2023.103056, 2023.

Cushman-Roisin, B. and Korotenko, K. A.: Mesoscale-resolving simulations of summer and winter bora events in the Adriatic Sea, J. Geophys. Res.-Oceans, 112, C11S91, https://doi.org/10.1029/2006JC003516, 2007.

Denamiel, C., Tojčić, I., and Vilibić, I.: Balancing accuracy and efficiency of atmospheric models in the northern Adriatic during severe bora events, J. Geophys. Res.-Atmos., 126, e2020JD033516, https://doi.org/10.1029/2020JD033516, 2021.

Fach, B. A., Orek, H., Yilmaz, E., Tezcan, D., Salihoglu, I., Salihoglu, B., et al.: Water mass variability and Levantine Intermediate Water formation in the Eastern Mediterranean between 2015 and 2017, J. Geophys. Res.-Oceans, 126, e2020JC016472, https://doi.org/10.1029/2020JC016472, 2021.

Gačić, M., Civitarese, G., Miserocchi, S., Cardin, V., Crise, A., and Mauri, E.: The open-ocean convection in the Southern Adriatic: a controlling mechanism of the spring phytoplankton bloom, Cont. Shelf Res., 22, 1897–1908, https://doi.org/10.1016/S0278-4343(02)00050-X, 2002.

Gačić, M., Borzelli, G. L. E., Civitarese, G., Cardin, V., and Yari, S.: Can internal processes sustain reversals of the ocean upper circulation? The Ionian Sea example, Geophys. Res. Lett., 37, L09608, https://doi.org/10.1029/2010GL043216, 2010.

GEBCO Compilation Group: GEBCO 2024 Grid, British Oceanographic Data Centre, https://doi.org/10.5285/1c44ce99-0a0d-5f4f-e063-7086abc0ea0f, 2024.

Haberle, I., Hackenberger, D. K., Djerdj, T., Bavčević, L., Geček, S., Hackenberger, B. K., et al.: Effects of climate change on gilthead seabream aquaculture in the Mediterranean, Aquaculture, 578, 740052, https://doi.org/10.1016/j.aquaculture.2023.740052, 2024.

Holt, J., Katavouta, A., Hopkins, J., Amoudry, L. O., Appendini, C. M., Arneborg, L., et al.: Future climate projections in the global coastal ocean, Prog. Oceanogr., 235, 103497, https://doi.org/10.1016/j.pocean.2025.103497, 2025.

Ingrosso, G., Bensi, M., Cardin, V., and Giani, M.: Anthropogenic CO2 in a dense water formation area of the Mediterranean Sea, Deep-Sea Res. Part I, 123, 118–128, https://doi.org/10.1016/j.dsr.2017.04.004, 2017.

IOC, SCOR and IAPSO: The international thermodynamic equation of seawater – 2010: Calculation and use of thermodynamic properties, IOC Manuals and Guides No. 56, UNESCO, Paris, https://doi.org/10.25607/OBP-1662, 2010.

Jacox, M. G. and Edwards, C. A.: Effects of stratification and shelf slope on nutrient supply in coastal upwelling regions, J. Geophys. Res.-Oceans, 116, C03019, https://doi.org/10.1029/2010JC006547, 2011.

Juza, M., Fernández-Mora, À., Tintoré, J.: Sub-regional marine heat waves in the Mediterranean Sea from observations: long-term surface changes, sub-surface and coastal responses, Front. Mar. Sci., 9, 785771, https://doi.org/10.3389/fmars.2022.785771, 2022.

Kamberi, E., Hala, E., and Möllmann, C.: Evidence of climate-driven regime shifts in Adriatic Sea fisheries, Sci. Mar., 89, e108, https://doi.org/10.3989/scimar.05566.108, 2025.

Kružić, P., Rodić, P., Popijač, A., and Sertić, M.: Impacts of temperature anomalies on mortality of benthic organisms in the Adriatic Sea, Mar. Ecol., 37, 1190–1209, https://doi.org/10.1111/maec.12293, 2016.

Kubin, E., Poulain, P.-M., Mauri, E., Menna, M., and Notarstefano, G.: Levantine intermediate and Levantine deep water formation: an Argo float study from 2001 to 2017, Water, 11, 1781, https://doi.org/10.3390/w11091781, 2019.

Kunze, E.: Limits on growing, finite-length salt fingers: a Richardson number constraint, J. Mar. Res., 45, 533–556, https://doi.org/10.1357/002224087788326885, 1987.

Le Meur, J., Wirth, A., de Mendoza, F. P., Miserocchi, S., and Cardin, V.: Intermittent supply of dense water to the deep South Adriatic Pit: an observational study, Front. Mar. Sci., 12, 1516780, https://doi.org/10.3389/fmars.2025.1516780, 2025.

Manca, B. B., Burca, M., Giorgetti, A., Coatanoan, C., Garcia, M. J., and Iona, A.: Physical and biochemical averaged vertical profiles in the Mediterranean regions: an important tool to trace the climatology of water masses and to validate incoming data from operational oceanography, J. Mar. Syst., 48, 83–116, https://doi.org/10.1016/j.jmarsys.2003.11.025, 2004.

Marini, M., Russo, A., Paschini, E., Grilli, F., and Campanelli, A.: Short-term physical and chemical variations in the bottom water of middle Adriatic depressions, Clim. Res., 31, 227–237, https://doi.org/10.3354/cr031227, 2006.

Martellucci, R., Dentico, C., Coppola, L., Skjelvan, I., Giani, M., Pensieri, S., et al.: Air–sea CO2 exchange in the Eastern Atlantic and the Mediterranean Sea based on autonomous surface measurements, Front. Mar. Sci., 12, 1633617, https://doi.org/10.3389/fmars.2025.1633617, 2025b.

Martinelli, M., Zacchetti, L., Belardinelli, A., Domenichetti, F., Scarpini, P., Penna, P., et al.: Changes in abundance and distribution of the sea pen, Funiculina quadrangularis, in the central Adriatic Sea (Mediterranean basin) in response to variations in trawling intensity, Fishes, 8, 347, https://doi.org/10.3390/fishes8070347, 2023.

Matić-Skoko, S., Pavičić, M., Šepić, J., Janeković, I., Vrdoljak, D., Vilibić, I., et al.: Impacts of sea bottom temperature on CPUE of European lobster Homarus gammarus (Linnaeus, 1758; Decapoda, Nephropidae) in the Eastern Adriatic Sea, Front. Mar. Sci., 9, 891197, https://doi.org/10.3389/fmars.2022.891197, 2022.

Maze, G. and Balem, K.: argopy: A Python library for Argo ocean data analysis, J. Open Source Softw., 5, 2425, https://doi.org/10.21105/joss.02425, 2020.

Mihanović, H., Vilibić, I., Carniel, S., Tudor, M., Russo, A., Bergamasco, A., et al.: Exceptional dense water formation on the Adriatic shelf in the winter of 2012, Ocean Sci., 9, 561–572, https://doi.org/10.5194/os-9-561-2013, 2013.

Mihanović, H., Vilibić, I., Šepić, J., Matić, F., Ljubešić, Z., Mauri, E., et al.: Observation, preconditioning and recurrence of exceptionally high salinities in the Adriatic Sea, Front. Mar. Sci., 8, 672210, https://doi.org/10.3389/fmars.2021.672210, 2021.

Mohamed, B. and Skliris, N.: Steric and atmospheric contributions to interannual sea level variability in the eastern Mediterranean Sea over 1993-2019, Oceanologia, 64, 50-62, https://doi.org/10.1016/j.oceano.2021.09.001, 2022.

Ozer, T., Rahav, E., Gertman, I., Sisma-Ventura, G., Silverman, J., and Herut, B.: Relationship between thermohaline and biochemical patterns in the Levantine upper and intermediate water masses, Southeastern Mediterranean Sea (2013–2021), Front. Mar. Sci., 9, 958924, https://doi.org/10.3389/fmars.2022.958924, 2022.

Pranić, P., Denamiel, C., Janeković, I., and Vilibić, I.: Multi-model analysis of the Adriatic dense-water dynamics, Ocean Sci., 19, 649–670, https://doi.org/10.5194/os-19-649-2023, 2023.

Querin, S., Bensi, M., Cardin, V., Solidoro, C., Bacer, S., Mariotti, L., et al.: Saw-tooth modulation of the deep-water thermohaline properties in the southern Adriatic Sea, J. Geophys. Res.-Oceans, 121, 4585–4600, https://doi.org/10.1002/2015JC011522, 2016.

Reich, T., Belkin, N., Sisma-Ventura, G., Hauzer, H., Berman-Frank, I., and Rahav, E.: Does oligotrophy favor chemoautotrophy over photoautotrophy?, Prog. Oceanogr., 241, 103633, https://doi.org/10.1016/j.pocean.2025.103633, 2026.

Richardson, C. M., Peucker-Ehrenbrink, B., Wyatt, S., Bourbonnais, A., Hatje, V., Frey, C., et al.: Effects of climate change on river and groundwater nutrient inputs to the coastal ocean, Commun. Earth Environ., 6, 761, https://doi.org/10.1038/s43247-025-02594-6, 2025.

Roether, W., Manca, B. B., Klein, B., Bregant, D., Georgopoulos, D., Beitzel, V., et al.: Recent changes in eastern Mediterranean deep waters, Science, 271, 333–335, https://doi.org/10.1126/science.271.5247.333, 1996.

Schlitzer, R., Roether, W., Oster, H., Junghaus, H.-G., Hausmann, M., Johannsen, H., et al.: Chlorofluoromethane and oxygen in the Eastern Mediterranean, Deep-Sea Res., 38, 1531–1551, https://doi.org/10.1016/0198-0149(91)90088-W, 1991.

Schmitt, R. W.: Double diffusion in oceanography, Annu. Rev. Fluid Mech., 26, 255-285, https://doi.org/10.1146/annurev.fl.26.010194.001351, 1994.

Schroeder, K. and Chiggiato, J. (Eds.): Oceanography of the Mediterranean Sea: An Introductory Guide, Elsevier, Amsterdam, 558 pp., https://doi.org/10.1016/C2020-0-01415-3, 2022.

Schroeder, K., Chiggiato, J., Josey, S. A., Borghini, M., Aracri, S., and Sparnocchia, S.: Rapid response to climate change in a marginal sea, Sci. Rep., 7, 4065, https://doi.org/10.1038/s41598-017-04455-5, 2017.

SeaDataNet: Data quality control procedures, version 2.0, https://www.seadatanet.org/content/download/596/file/SeaDataNet_QC_procedures_V2_(May_2010).pdf, 2010.

Simoncelli, S., Schaap, D., and Schlitzer, R.: Mediterranean Sea – Temperature and salinity Historical Data Collection SeaDataCloud V2 (SDC_MED_DATA_TS_V2) [Dataset], SeaDataNet, https://doi.org/10.12770/2a2aa0c5-4054-4a62-a18b-3835b304fe64, 2020.

Skliris, N., Marsh, R., Breedon, M., and Josey, S. A.: Accelerated warming and salinification of the Mediterranean Sea: Implications for dense water formation, J. Mar. Sci. Eng., 13, 25, https://doi.org/10.3390/jmse13010025, 2025.

Terzić, E., Cardin, V., Le Meur, J., Dunić, N., Vodopivec, M., and Vilibić, I.: Unprecedented warming and salinization observed in the deep Adriatic, Limnol. Oceanogr. Lett., 10, 888–898, https://doi.org/10.1002/lol2.70051, 2025a.

Terzić, E., Gardiol, C., and Vilibić, I.: Surface saline lakes in the Mediterranean Sea, Ocean Sci., 21, 1441–1459, https://doi.org/10.5194/os-21-1441-2025, 2025b.

Terzić, E. and Vilibić, I.: Cleaned Adriatic in situ hydrographic data (1952–2023) for a Mediterranean thermohaline acceleration analysis [Dataset], Zenodo, https://doi.org/10.5281/zenodo.20345373, 2026a.

Terzić, E. and Vilibić, I.: MedClim analysis code for Mediterranean thermohaline acceleration analysis [Software], Zenodo, https://doi.org/10.5281/zenodo.20410481, 2026b.

Terzić, E. and Vilibić, I.: Observational evidence for accelerated warming and salinification propagating into the deep Mediterranean, Geophys. Res. Lett., 53, e2026GL124518, https://doi.org/10.1029/2026GL124518, 2026c.

Terzić, E. and Vilibić, I.: Analysis code for “Recent thermohaline shifts in the Adriatic Sea and their potential consequences” [Software], Zenodo, https://doi.org/10.5281/zenodo.23016822, 2026d.

Tintoré, J., Pinardi, N., Álvarez-Fanjul, E., Aguiar, E., Álvarez-Berastegui, D., Bajo, M., et al.: Challenges for sustained observing and forecasting systems in the Mediterranean Sea, Front. Mar. Sci., 6, 568, https://doi.org/10.3389/fmars.2019.00568, 2019.

Verri, G., Furnari, L., Gunduz, M., Senatore, A., Santos da Costa, V., De Lorenzis, A., et al.: Climate projections of the Adriatic Sea: role of river release, Front. Climate, 6, 1368413, https://doi.org/10.3389/fclim.2024.1368413, 2024.

Vilibić, I., Matijević, S., Šepić, J. and Kušpilić, G.: Changes in the Adriatic oceanographic properties induced by the Eastern Mediterranean Transient, Biogeosci., 9, 2085–2097, https://doi.org/10.5194/bg-9-2085-2012, 2012.

Vilibić, I., Zemunik, P., Šepić, J., Dunić, N., Marzouk, O., Mihanović, H., et al.: Present-climate trends and variability in thermohaline properties of the northern Adriatic shelf, Ocean Sci., 15, 1351–1362, https://doi.org/10.5194/os-15-1351-2019, 2019.

Vilibić, I., Pranić, P. and Denamiel, C.: North Adriatic Dense Water: lessons learned since the pioneering work of Mira Zore-Armanda 60 years ago, Acta Adriat., 64, 53–78, https://doi.org/10.32582/aa.64.1.11, 2023.

Wagawa, T., Igeta, Y. and Abe, S.: Warming and springtime freshening trend in the southeastern Sea of Japan revealed by observational data, Geophys. Res. Lett., 52, e2025GL118631, https://doi.org/10.1029/2025GL118631, 2025.

Wang, G., Cheng, L., Boyer, T., and Li, C.: Halosteric sea level changes during the Argo era, Water, 9, 484, https://doi.org/10.3390/w9070484, 2017.

Wong, A., Keeley, R., and Carval, T., and the Argo Management Team: Argo Quality Control Manual for CTD and Trajectory Data. Version 3.7. https://doi.org/10.13155/33951, 2023.

Zore-Armanda, M.: Les masses d'eau de la mer Adriatique, Acta Adriat., 10, 5–88, 1963.

Zore-Armanda, M., Bone, M., Dadić, V., Morović, M., Ratković, D., Stojanoski, L., and Vukadin, I.: Hydrographic properties of the Adriatic Sea in the period from 1971 through 1983, Acta Adriat., 32, 1–547, 1991.

Table 1. Observational dataset inventory. Counts are retained casts entering the climatologies behind Figs. 1–2. DJ1 and DJ3 are the northern and southern Adriatic polygons, labelled after the sub-basin nomenclature of Manca et al. (2004); they follow the coastline and bathymetry rather than that paper's boundaries (Sect. 2.2), so their bounding boxes are given in (d). In (b), note the 20th-century summer count in DJ3 (444), the sparsest season–period combination. In (e), the shallowest bin centre of 5 m spans the layer in which the two periods are sampled least alike, and is not interpreted in summer (Sect. 3.1). SeaDataNet counts exclude the float profiles held by the Argo set and include the thermosalinograph records (Sect. 2.1). Sources: RBI, Ruđer Bošković Institute; IOR, Institute of Oceanography and Fisheries; MSFD, conductivity–temperature–depth (CTD) casts of the Croatian national monitoring programme under the Marine Strategy Framework Directive; Argo, profiling floats. Seasons: JFM, January–March; AMJ, April–June; JAS, July–September; OND, October–December.

(a) Casts by source, region and period

Region	Source	1950–1999	2000–2025	Total
DJ1	SeaDataNet	8903	11014	19917
DJ1	RBI northern Adriatic transect 1979–2017	984	1037	2021
DJ1	IOR Adriatic database 1987–2019	731	829	1560
DJ1	Croatian MSFD monitoring CTD 2019–2023	0	429	429
DJ1	Argo	0	293	293
DJ3	SeaDataNet	3291	2647	5938
DJ3	Argo	0	2946	2946
DJ3	IOR Adriatic database 1987–2019	141	323	464
DJ3	Croatian MSFD monitoring CTD 2019–2023	0	96	96

(b) Casts by season

Region	Period	JFM	AMJ	JAS	OND	Total
DJ1	1950–1999	1946	2726	3847	2099	10618
DJ1	2000–2025	3388	2639	4104	3471	13602
DJ3	1950–1999	1028	1163	444	797	3432
DJ3	2000–2025	1079	1478	1708	1747	6012

(c) Casts by maximum depth reached [m]

Region	Period	0–50	50–200	200–600	600–1000	$\geq$1000
DJ1	1950–1999	9931	687	0	0	0
DJ1	2000–2025	12697	905	0	0	0
DJ3	1950–1999	151	1009	804	1076	392
DJ3	2000–2025	1171	829	850	2258	904

(d) Region boundaries (polygon bounding box)

Region	Name	Longitude	Latitude
DJ1	Northern Adriatic	12.065–15.538 °E	43.623–45.809 °N
DJ3	Southern Adriatic	15.888–20.021 °E	39.790–42.940 °N

(e) Processing parameters

Bin centres (m): 5, 10, 20, 30, 40, 50, 75, 100, 125, 150, 200, 250, 300, 400, 500, 600, 700, 800, 900, 1000, 1100, 1200. Minimum fractional coverage per level: 0.05 (both T and S). Second-pass outlier rejection: 1.0 standard deviation. Accepted quality flags: 1 and 2 (SeaDataNet and Argo). Equation of state: TEOS-10; σ_0 referenced to 0 dbar.

Table 2. Warming and salinification rates for 2000–2025 in the Adriatic and in the rest of the Mediterranean, computed with the same method on both sides (Sect. 2.4). Mediterranean values (Med.) are the median over the depth bins of the layer in the 25 sub-basins outside the Adriatic, with their interquartile range (IQR); Adriatic values are the median over the depth bins of the layer. A trend is reported only where the series holds at least 36 monthly values and the 2000–2025 window at least 24 (Sect. 2.4). Ratios are computed from the unrounded rates. DJ1 is reported only to 50 m, because only 905 of its 13 602 casts reach 50 m or deeper (Sect. 2.3). Above 200 m the DJ3 ratios depend on the cast population: on casts over water deeper than 800 m the temperature ratios are 0.79 and 0.86, not distinguishable from one, and the salinity ratios 3.4 and 2.1 (Sect. 3.3).

Variable	Layer	DJ1	DJ3	Med.	Med. IQR	DJ1/Med	DJ3/Med
T [°C decade^{-1}]	5–50 m	$+0.600$	$+0.220$	$+0.404$	$+0.265$ to $+0.510$	1.5	0.55
T	75–200 m	—	$+0.249$	$+0.344$	$+0.270$ to $+0.400$	—	0.72
T	250–600 m	—	$+0.334$	$+0.222$	$+0.165$ to $+0.290$	—	1.5
T	700–1200 m	—	$+0.429$	$+0.070$	$+0.037$ to $+0.110$	—	**6.2**
S [decade^{-1}]	5–50 m	$+0.154$	$+0.224$	$+0.052$	-0.032 to $+0.095$	2.9	**4.3**
S	75–200 m	—	$+0.101$	$+0.076$	$+0.022$ to $+0.113$	—	1.3
S	250–600 m	—	$+0.126$	$+0.067$	$+0.055$ to $+0.083$	—	1.9
S	700–1200 m	—	$+0.122$	$+0.033$	$+0.014$ to $+0.044$	—	**3.7**

Table 3. Steric sea level trends in the Southern Adriatic Pit, 2014–2024, from deseasoned monthly means of Argo profiles. Intervals are 95 % confidence intervals on the trend; they are not standard deviations of the underlying series. Because successive monthly values are correlated, the number of independent values is much smaller than the number of months, and the intervals are correspondingly wide (Sect. 2.8). Eastern Mediterranean values are from Mohamed and Skliris (2022) for 1993–2019 and are shown on their own integration layer.

Layer / source	Thermosteric [mm yr^{-1}]	Halosteric [mm yr^{-1}]	Net [mm yr^{-1}]
This study, 0–1000 m	$\mathbf{+9.80 \pm 2.71}$	$\mathbf{-15.21 \pm 2.33}$	$\mathbf{-5.41 \pm 2.49}$
This study, 0–700 m	$+5.30 \pm 2.19$	-11.03 ± 2.54	-5.73 ± 2.28
This study, 0–400 m	$+2.26 \pm 1.37$	-6.81 ± 2.55	-4.55 ± 1.73
This study, 600–1000 m	$+5.7 \pm 0.9$	-5.6 ± 1.0	$+0.1 \pm 0.5$
Eastern Mediterranean, 0–400 m, 1993–2019	$+2.13 \pm 0.41$	-0.75 ± 0.19	—

Table 4. Argo floats contributing to the Southern Adriatic Pit analyses (steric decomposition and double-diffusive diagnostics, Sects. 2.8–2.9), restricted to ascending profiles reaching at least 1000 dbar.

WMO	Profiles	First	Last	Max. pressure [dbar]
1900848	13	2010-04	2014-04	1184.6
3901978	16	2018-10	2019-09	1220.9
3902626	50	2024-12	2025-11	1227.0
6900979	8	2013-08	2013-11	1173.0
6901040	25	2012-03	2014-05	1216.0
6901822	100	2013-03	2017-12	1227.9
6901827	68	2013-09	2018-05	1207.6
6901862	6	2015-03	2015-04	1018.4
6902848	46	2020-04	2022-11	1223.9
6903178	65	2015-10	2016-08	1222.7
6903197	27	2016-04	2017-02	1016.5
6903236	3	2018-11	2018-11	1213.3
6903250	57	2018-10	2021-01	1020.9
6903781	8	2020-07	2021-01	1228.0
6903799	181	2021-05	2025-12	1230.8
6903821	12	2024-07	2025-01	1151.3
6903825	42	2022-12	2025-12	1017.8
7902334	30	2025-09	2025-12	1215.5

Table 5. Salt-finger diagnostics by layer in the Southern Adriatic Pit, from 757 Argo profiles divided into those taken before 2017 (257 profiles) and those taken from 2017 onward (500 profiles). Layers are the classical 200–400 m LIW salinity-maximum range (Sect. 3.4), the 400–600 m layer immediately below it, and the deep layer. Extent is the percentage of levels in the salt-finger regime, vigour the percentage of those levels with $R_\rho < 2$, and N^2 the squared buoyancy frequency. Extent and vigour are means across profiles, N^2 is the median across profiles of each profile's median over its statically stable levels, and p-values are two-sided Mann–Whitney tests on the per-profile layer statistics; those below 0.05 are in bold. On annual means, only the vigour and the N^2 of the deep layer differ significantly between the periods (Sect. 3.7). The last row is the 350–550 m layer instrumented at the EMSO-E2M3A mooring, given only so that our diagnostics can be compared with Amorim et al. (2024) in Sect. 4.2; it straddles the base of the core and is not one of our layers.

	Extent [%]			Vigour [%]			N^2 [10^{-6} s^{-2}]		
Layer	<2017	≥2017	p	<2017	≥2017	p	<2017	≥2017	p
200–400 m *(LIW core)*	55.3	56.0	0.93	34.6	32.3	0.17	1.96	1.64	$\mathbf{3 \times 10^{-5}}$
400–600 m	56.6	60.3	**0.029**	28.0	39.0	$\mathbf{4 \times 10^{-9}}$	2.50	1.10	$\mathbf{3 \times 10^{-38}}$
600–1000 m	92.1	87.7	$\mathbf{7 \times 10^{-29}}$	10.7	37.4	$\mathbf{7 \times 10^{-81}}$	2.55	1.73	$\mathbf{3 \times 10^{-94}}$
350–550 m (mooring layer)	*48.6*	*56.9*	$\mathbf{1 \times 10^{-7}}$	*29.1*	*36.9*	$\mathbf{2 \times 10^{-5}}$	*2.51*	*1.04*	$\mathbf{8 \times 10^{-35}}$

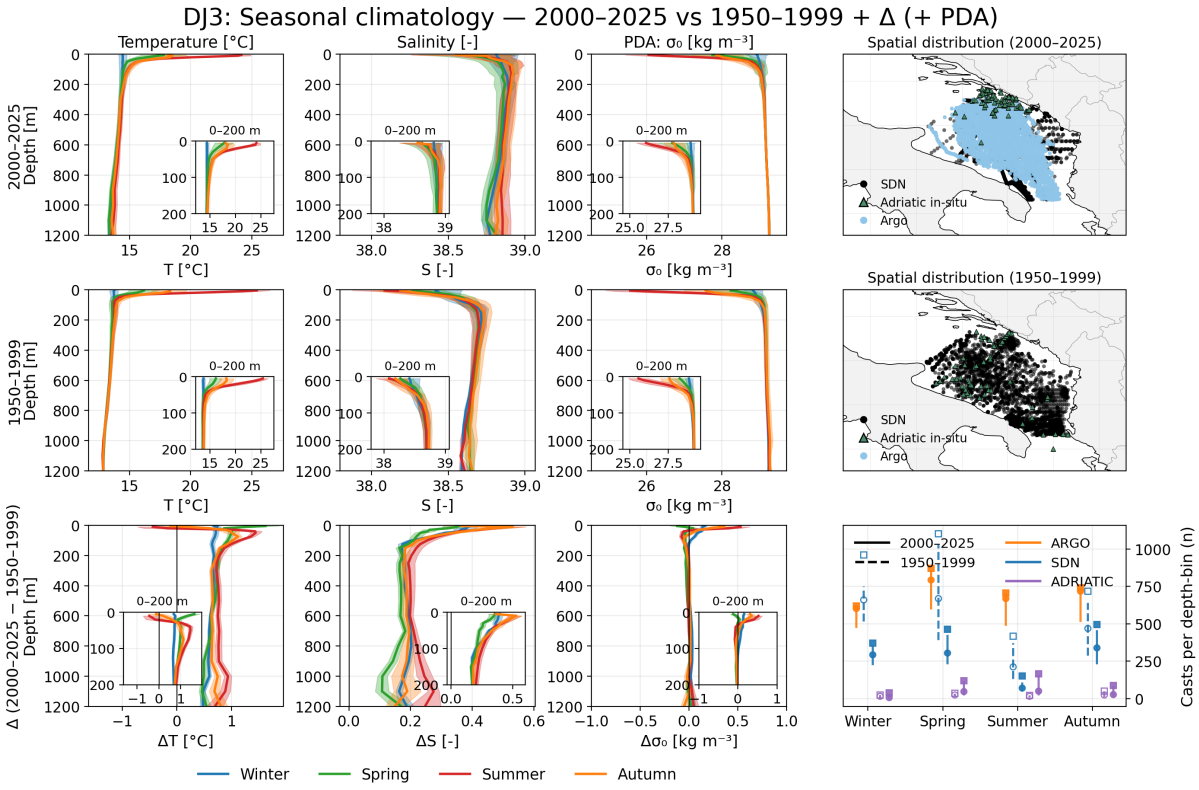


Figure 1. Seasonal climatology of the southern Adriatic (DJ3, Sect. 2.2) from all available in situ sources. Rows: 2000–2025 (top), 1950–1999 (middle), and their difference (bottom); columns: temperature, salinity, potential density anomaly and, on the right, the sampling behind them. Colours denote seasons. Insets expand the upper 200 m. In the two period rows the shading is ± 1 standard deviation, the spread of the observations contributing to each level. In the difference row it is the 95 % confidence interval on the difference, computed with all casts of one cruise-day counted as a single independent observation (Sect. 2.3). The 5 m summer bin is omitted from the difference row because the two periods sample that level differently, and the summer differences at 10 and 20 m are shown but not interpreted (Sect. 3.1). The right column shows the spatial distribution of casts by source for each period (top two rows) and the number of casts per depth bin by source and season (bottom row; for SeaDataNet its CTD, bottle and bathythermograph casts): maxima over the depth bins as squares, medians as circles and interquartile ranges across the depth bins as vertical lines, solid for 2000–2025 and dashed for 1950–1999.

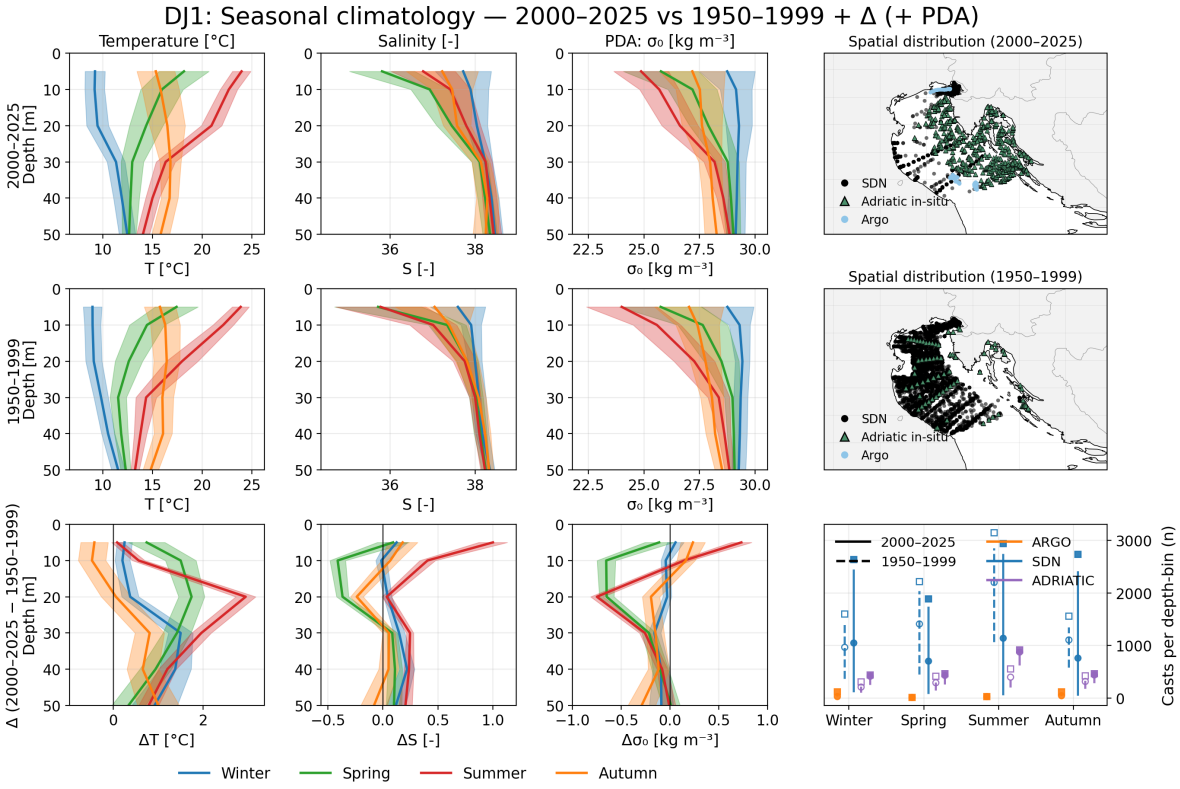


Figure 2. As Fig. 1, but for the northern Adriatic (DJ1, Sect. 2.2) and restricted to 0–50 m. Below 50 m the northern shelf carries 687 and 905 casts in the two periods against 9931 and 12 697 above it (Table 1), and the fitted trend changes sign with the analysis window, so deeper levels are not shown. Confidence intervals are wider relative to the signal than in Fig. 1 because cast clustering within cruises is stronger on the shelf, with variance inflation factors of 5.5–6.2 against 1.9–2.4 in the south for 2000–2025 (6.7–7.6 against 3.6–5.7 for 1950–1999).

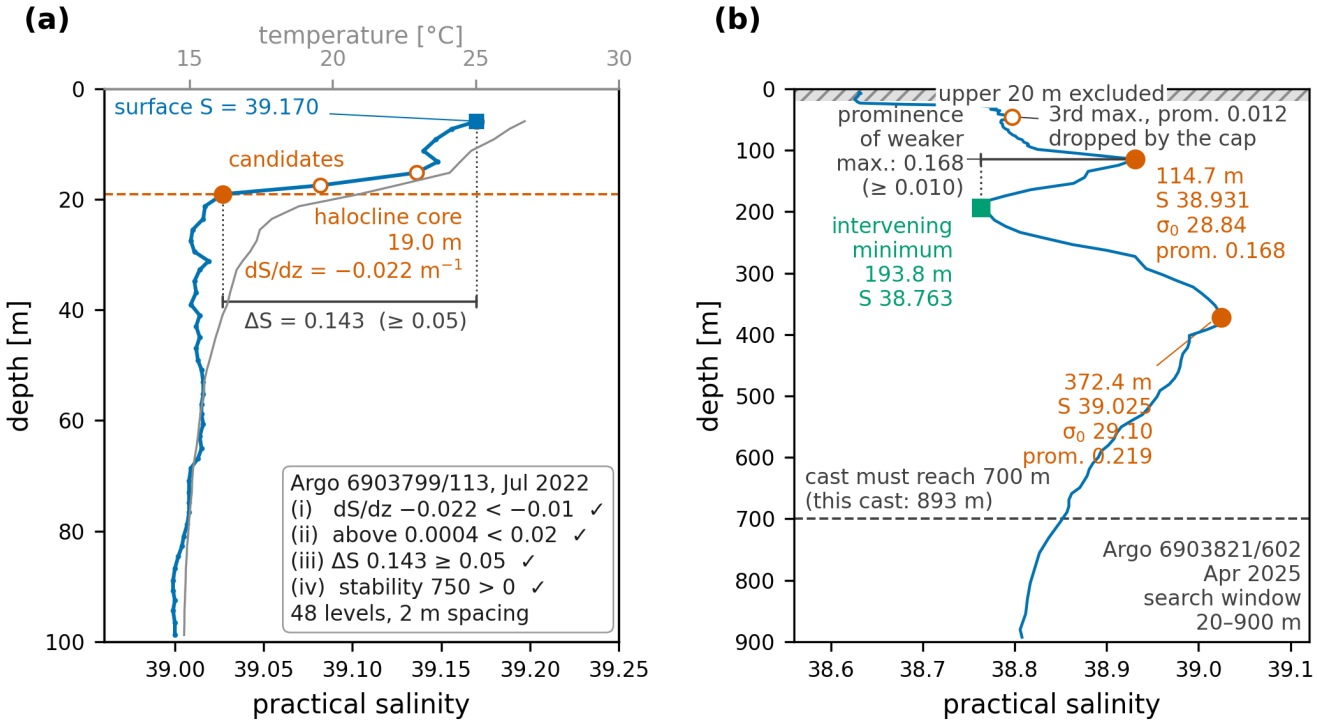


Figure 3. The two detection criteria of Sects. 2.6 and 2.7 applied to measured profiles. **(a)** Surface saline lake: Argo float 6903799, cycle 113, 26 July 2022, practical salinity (blue) and temperature (grey) over 0–100 m. Open circles mark the levels at which the salinity gradient falls below $-0.01\,\mathrm{m}^{-1}$; the halocline core (filled circle and dashed line) is the candidate nearest 100 m, here at 19.0 m with a gradient of $-0.022\,\mathrm{m}^{-1}$. The bracket is the salinity contrast between the first sampled level (5.9 m) and the core, 0.143 against the threshold of 0.05, and the box lists the four criteria with their values for this profile. **(b)** Double salinity maximum: Argo float 6903821, cycle 602, 11 April 2025, practical salinity over 0–900 m. Filled circles are the two maxima retained, at 114.7 and 372.4 m; the square is the minimum between them, down to which the prominence of the weaker maximum (0.168, horizontal bracket) is measured; the open circle is a third, weaker maximum (prominence 0.012) removed by the two-per-cast cap. The upper 20 m are excluded from the search (hatched) and only casts reaching 700 m (dashed line) enter the frequency statistics.

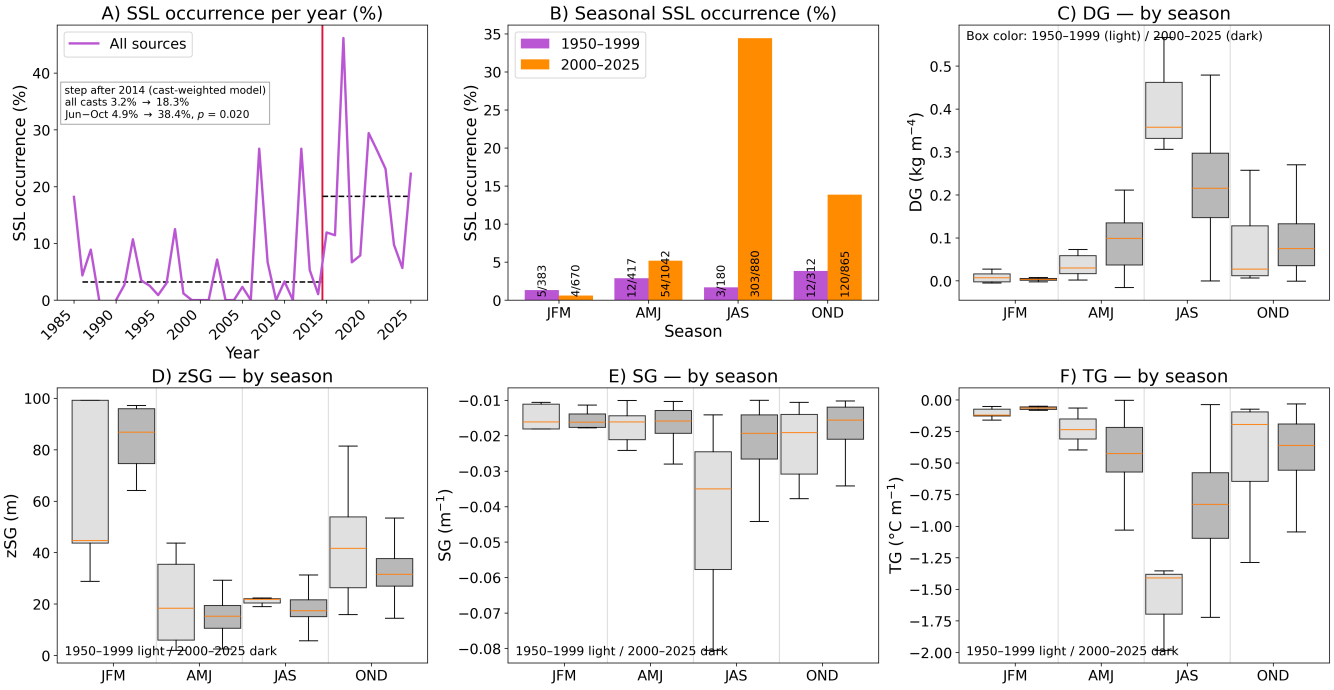


Figure 4. Surface saline lakes in the southern Adriatic, restricted to resolution-matched casts: median level spacing ≤ 5 m and at least 8 levels in 0–100 m, computed per cast from the source profiles. **(A)** Annual occurrence among evaluated casts, shown for every year with at least one matched cast; the red line marks the step found by the change-point model of Sect. 2.5, after 2014, and the dashed lines the occurrence pooled over all matched casts before and after it (3.2 and 18.3 %). The test is made on the casts, not on these annual values. **(B)** Seasonal occurrence by period, annotated with detections over evaluated casts. **(C–F)** Seasonal distributions of the density gradient, core depth, salinity gradient and temperature gradient of the SSL core, for detected events only, light boxes for 1950–1999 and dark for 2000–2025. Restricting to matched casts is essential: at historical bottle spacing the detection criteria return nothing at all (Fig. A1). The 1950–1999 summer boxes in (C–F) rest on the three matched detections of that season and period (panel B) and should not be read as distributions.

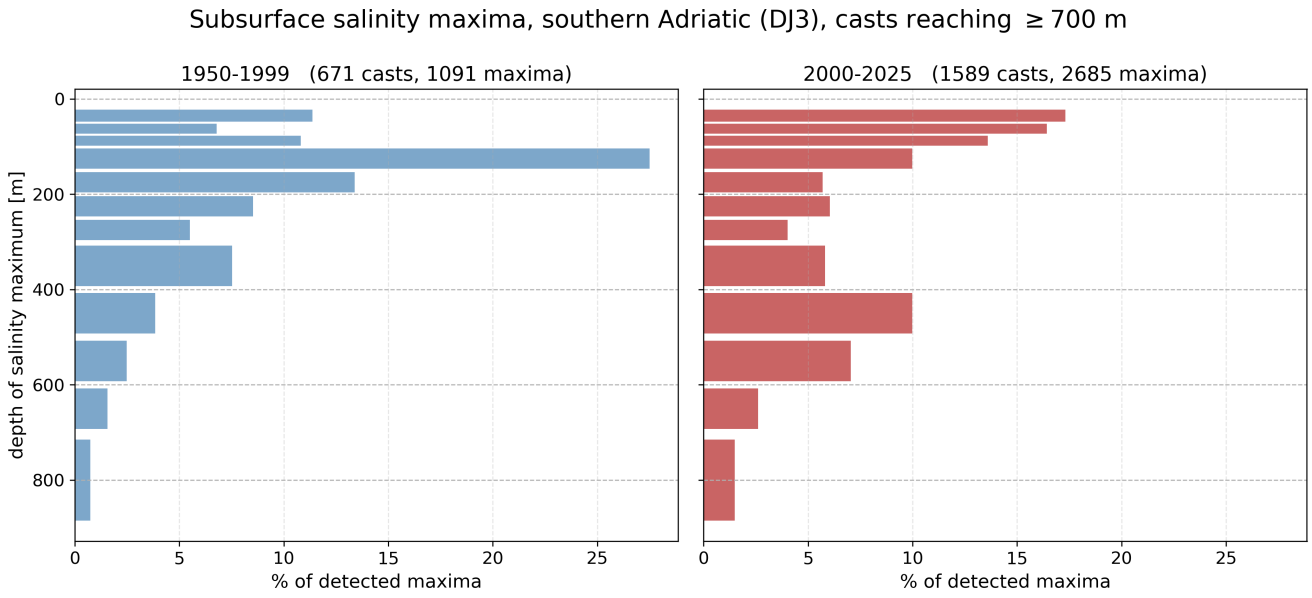


Figure 5. Subsurface salinity maxima in the southern Adriatic, detected individually in each cast by peak prominence, for 1950–1999 and 2000–2025. Only casts reaching 700 m are used, which alone can resolve both features; neighbouring maxima not separated by a salinity dip of at least 0.010 are counted as one, and only the two most prominent maxima of each cast are retained. A cast carrying a single maximum contributes one detection, which is why the number of maxima is less than twice the number of casts. The cap is needed because at a prominence threshold of 0.010 a small number of very high-resolution historical casts return hundreds of peaks each, and fifteen such casts would otherwise supply more than half of all 1950–1999 detections among casts reaching 700 m. Depth bins are 20–50, 50–75 and 75–100 m, then 50 m wide to 300 m, 100 m wide to 700 m and a single bin for 700–900 m. In 1950–1999 the maxima concentrate in one band, 27 % of them in the single 100–150 m interval and 41 % within 100–200 m; in 2000–2025 that band holds 16 % and the detections concentrate above 100 m, with a second mode at 400–600 m. The historical distribution is what a single-core description of the intermediate layer represents; the modern one is not. Detection is on native vertical resolution; the degraded-resolution repeat is reported in Sect. 3.4. Panels share a common horizontal scale.

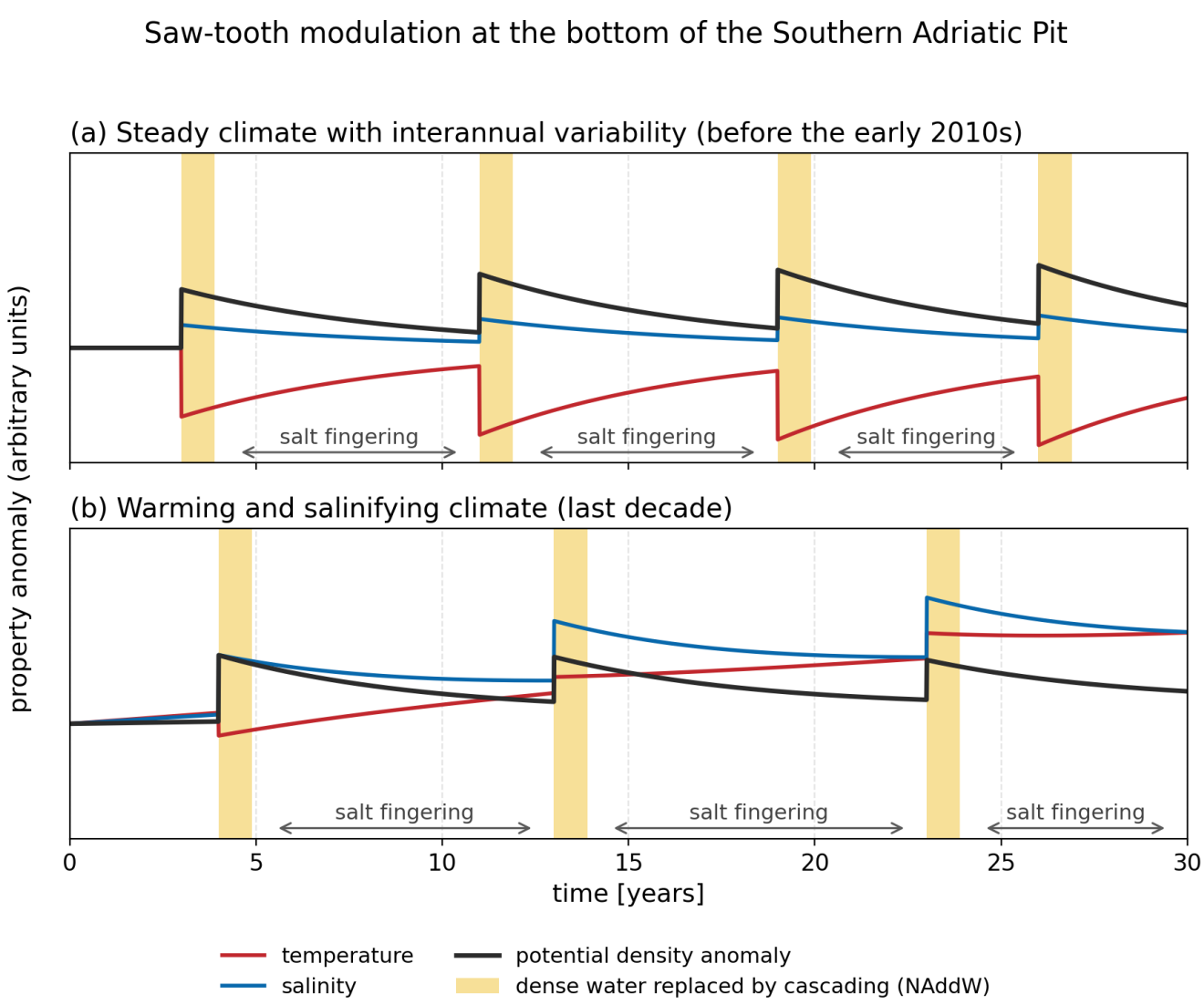


Figure 6. Schematic saw-tooth modulation of temperature, salinity and potential density anomaly at the bottom of the Southern Adriatic Pit. Panel (a) follows the saw-tooth described by Querin et al. (2016); panel (b) sketches how it is modified under the recent regime. **(a)** Steady climate with interannual variability, before the early 2010s: each cascading event delivers cold water, so density rises mainly through the thermal term and properties differ from year to year. **(b)** Warming and salinifying climate of the last decade (Terzić et al., 2025a): cascading water is only weakly cooled but much saltier, so the density step is smaller and the record carries an underlying warming and salinifying drift. The temperature step no longer has a fixed sign. The first event sketched here still cools the deep layer, while the later two bring water warmer than the water they replace, so an event can now raise deep temperature as well as lower it. Yellow bars mark the intervals during which resident deep water is replaced by cascading North Adriatic Dense Water; between them, properties relax under double-diffusive and other mixing. Salt fingering is marked over the relaxation phases only, and is intermittent because the density ratio rather than the Turner angle governs whether fingers transport salt appreciably (Sect. 3.7). Note that the figure is a schematic and not a data plot.

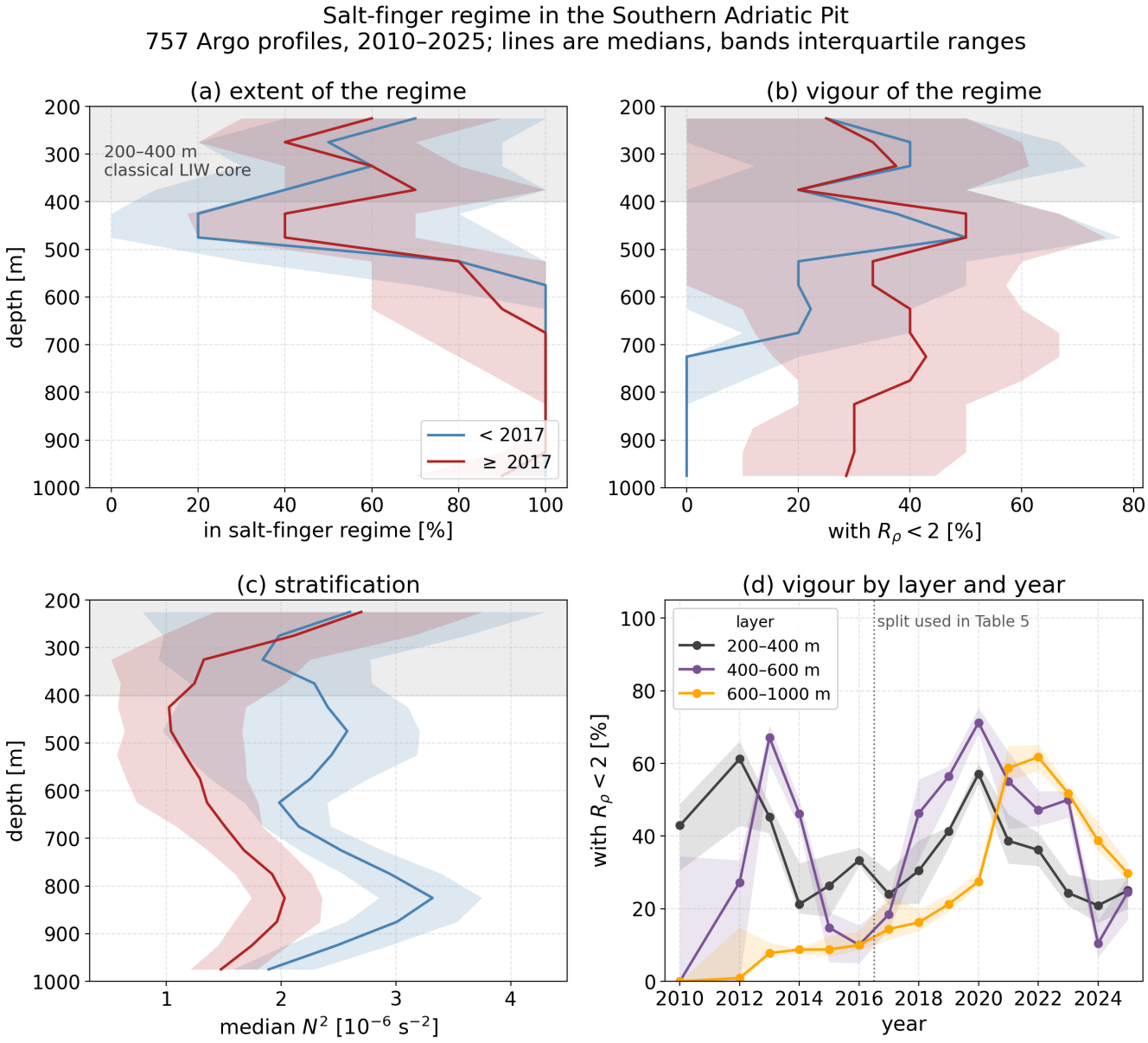


Figure 7. Salt-finger regime in the Southern Adriatic Pit from 757 Argo profiles, 2010–2025, divided into profiles taken before 2017 and from 2017 onward. Lines are medians across profiles within each 50 m depth bin, bands the interquartile range. **(a)** Fraction of each bin in the salt-finger regime: the extent of the regime. **(b)** Fraction of the finger-regime levels with density ratio $R_\rho < 2$, the range in which fingers grow fast enough to outrun internal-wave strain: the vigour of the regime. **(c)** Median N^2. The grey band marks the classical 200–400 m LIW salinity-maximum range. **(d)** The vigour of the regime in the three layers of Sect. 2.9, year by year: the median across profiles of the per-profile vigour, with a 95 % bootstrap band over profiles; years with fewer than eight profiles are omitted, and the dotted line marks the split used in Table 5. The deep layer rises from below 1 % in 2010–2012 to 59–62 % in 2021–2022 and relaxes to 30 % in 2025; the 400–600 m layer was already vigorous in 2013–2014, fell to 10–15 % in 2015–2016 and peaked again at 71 % in 2020; the core shows no trend. The layer means before and from 2017 are tabulated with their p-values in Table 5.

Appendix A: Supporting analyses

This appendix collects three analyses that support choices made in the main text. Figure A1 documents the vertical resolution of the southern Adriatic archive over time and the degradation experiment that justifies restricting the surface saline lake series to resolution-matched casts (Sects. 2.5 and 3.5). Figure A2 shows the steric time series behind Table 3 and the reason its confidence intervals are wide (Sect. 2.8). Figure A3 repeats the double-maximum detection of Sect. 3.4 across its free parameters, to show which conclusions hold under every setting (Sect. 2.7).

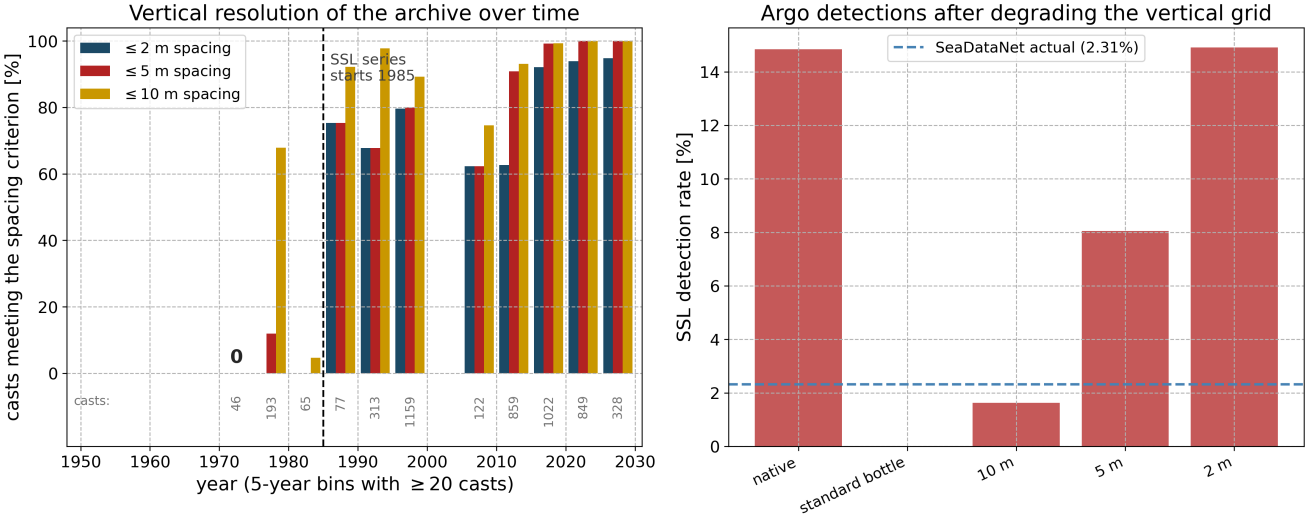


Figure A1. Vertical resolution of the southern Adriatic archive and its effect on surface saline lake detection. **Left:** the vertical resolution of the southern Adriatic archive itself (SeaDataNet and Argo casts; the IOR and monitoring casts are not shown), as the percentage of casts per five-year bin whose median level spacing in 0–100 m meets each criterion; bins with fewer than 20 casts are omitted. Bins are labelled with the number of casts behind them, and a bin whose bars are all zero is marked "0", so that an empty bin is not read as missing data. Before 1975 casts exist but none reaches even 10 m median spacing; the 1975–1979 casts are markedly better, 68 % of them at 10 m and 12 % at 5 m, but those fine casts carry too few levels to be evaluated (Sect. 2.6), which is why occurrence is plotted only from 1985 (dashed line). After 2015 almost every cast meets the 5 m resolution threshold. **Right:** the degradation experiment. Argo profiles are re-sampled onto progressively coarser vertical grids and the identical detection criteria re-applied. Detections are 437 (14.84 %) at native 1–5 m spacing and 439 at 2 m, and fall to 237 at 5 m and 48 at 10 m, in profiles that demonstrably contain a surface saline lake at native resolution; on the standard bottle grid (0, 10, 20, 30, 50, 75, 100 m) no profile can be evaluated, because the grid carries seven levels in the upper 100 m against the eight the detection requires. The dashed line is the detection rate among the SeaDataNet casts that carry at least eight levels in the upper 100 m (2.3 %).

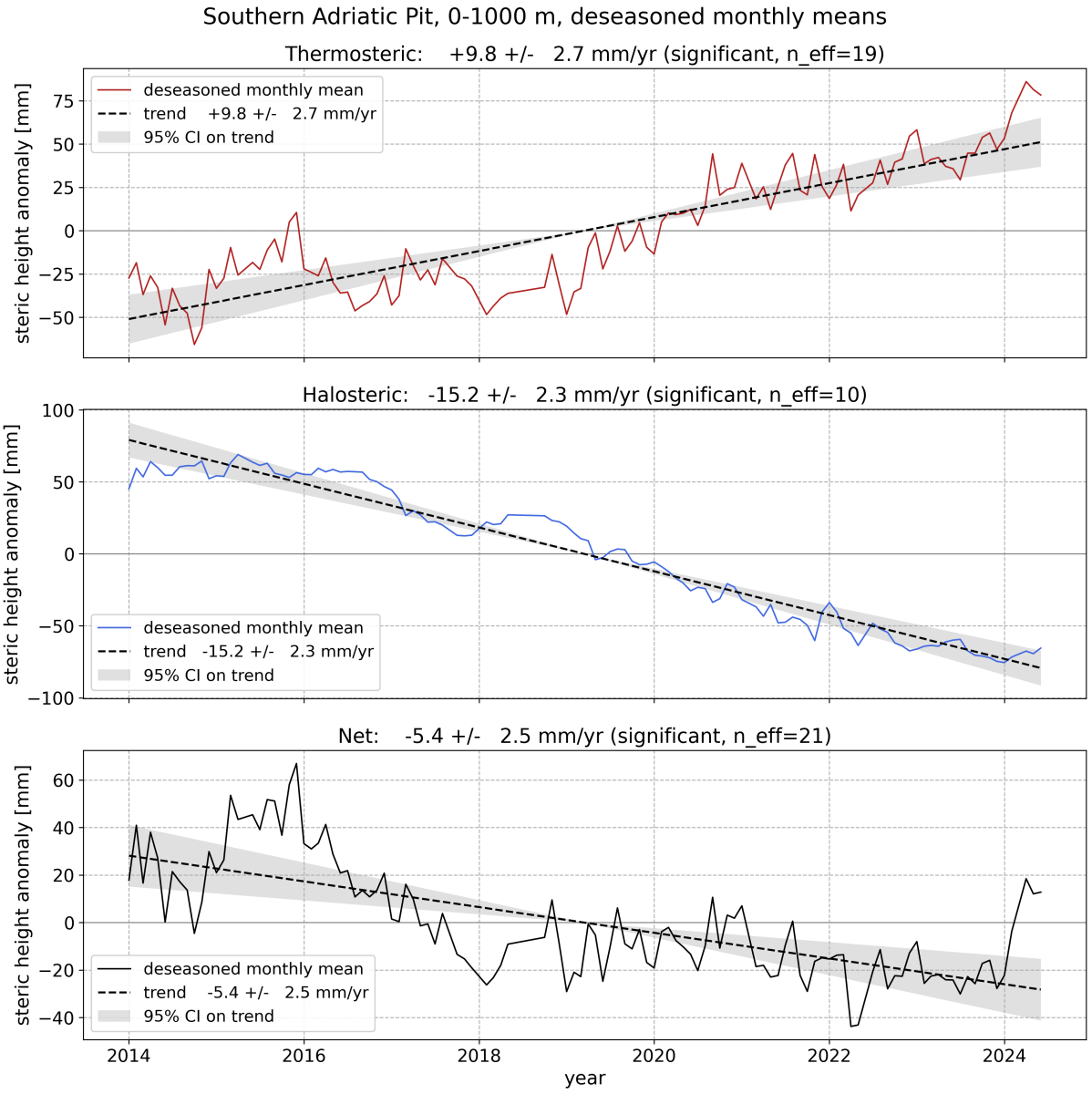


Figure A2. Thermosteric, halosteric and net steric height in the Southern Adriatic Pit over 2014–2024, the window of Table 3, from deseasoned monthly means on a common 0–1000 dbar grid, with fitted trends and 95 % confidence bands corrected for residual autocorrelation. Anomalies are shown about each series mean, so that the three panels are comparable. The window, January 2014 to June 2024, holds 116 monthly values, but successive months resemble one another (lag-1 correlation 0.7–0.8), so the effective sample size $n_{\mathrm{eff}} = n(1-r_1)/(1+r_1)$ behind each interval is only 10–21. The bands are wide for that reason, not because the monthly means are noisy.

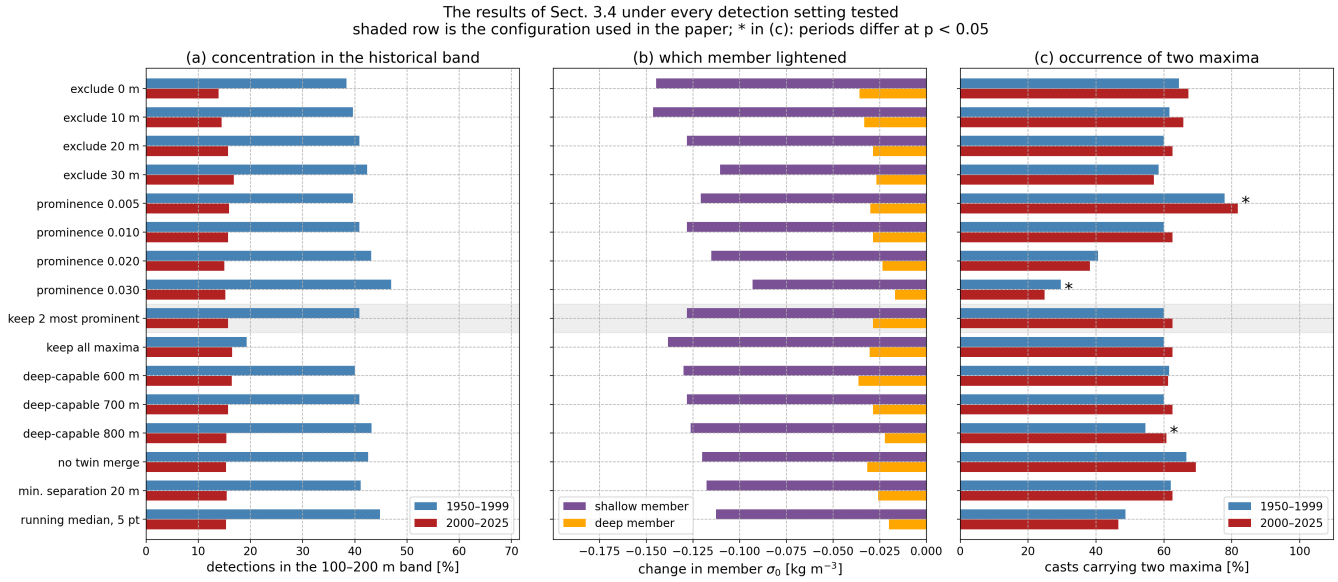


Figure A3. Sensitivity of the two results of Sect. 3.4 to the detection settings. The free choices (Sect. 2.7) are the depth above which maxima are ignored, the prominence threshold, whether all maxima or only the two most prominent are kept per cast, how deep a cast must reach to be used, and how noise on a salinity crest is treated: the paper counts neighbouring maxima as one unless the salinity dips by at least the prominence threshold between them, and the last three rows show no merging at all, a minimum separation of 20 m between retained maxima, and a five-point running median applied to each profile before detection. Each row varies one setting; the sixteen rows hold thirteen distinct configurations, because the configuration used in the paper (shaded) appears once in four of the five groups of settings. **(a)** Share of detected maxima falling in the 100–200 m band. It is higher in 1950–1999 than in 2000–2025 in all thirteen configurations: at 38.4–47.0 % against 13.9–16.8 % in the twelve that keep at most two maxima per cast, and at 19.3 against 16.5 % when all maxima are kept. **(b)** Change in σ_0 of each member between the periods. The shallower member lightens by 3.6 to 5.7 times as much as the deeper one, again in every configuration. **(c)** Share of casts carrying two maxima in each period; an asterisk marks a configuration in which the difference between the periods is significant ($p < 0.05$, chi-square). It rises in some configurations and falls in others, which is why no trend in it is claimed (Sect. 3.4).